An efficient Fourier spectral eigensolver for computing the Bogoliubov-de Gennes excitations of spin-1 Bose-Einstein condensates

Yu LI[a], Zhixuan LI[b], Manting XIE[c,*], Yong ZHANG[d]

[a]*Coordinated Innovation Center for Computable Modeling in Management Science,*
Tianjin University of Finance and Economics, Tianjin 300222, China
[b]*School of Mathematics, Sichuan University, Chengdu 610064, China*
[c]*School of Mathematics and KL-AAGDM, Tianjin University, Tianjin 300350, China*
[d]*Center for Applied Mathematics and KL-AAGDM, Tianjin University, Tianjin 300072, China*

Abstract

In this paper, we propose a spectrally accurate solver for computing the elementary/collective excitations of spin-1 Bose-Einstein condensates (BEC), which is governed by the Bogoliubov-de Gennes (BdG) equation, around the mean-field ground state. The BdG equation is essentially a constrained eigenvalue/eigenfunction system. Firstly, we investigate its analytical properties, including exact eigenpairs, generalized nullspace, and bi-orthogonality of eigenspaces. Secondly, by combining the standard Fourier spectral method for spatial discretization and a stable Gram-Schmidt bi-orthogonal algorithm, we develop a subspace iterative solver for such a large-scale dense eigenvalue problem, and it proves to be numerically stable, efficient, and accurate. Our solver is matrix-free and the operator-function evaluation is accelerated by discrete Fast Fourier Transform (FFT) with almost optimal efficiency. Therefore, it is memory-friendly and efficient for large-scale problems. Furthermore, we give a rigorous and detailed numerical analysis on the stability and spectral convergence. Finally, we present extensive numerical results to illustrate the spectral accuracy and efficiency, and investigate the excitation spectrum and Bogoliubov amplitudes around the ground state in 1–3 spatial dimensions.

Keywords: Spin-1 Bose-Einstein condensates, Bogoliubov-de Gennes excitations, Fourier spectral method, bi-orthogonal structure, large-scale problem

1. Introduction

Since the experiment realizations of degenerate spinor BEC with ultracold rubidium [14] and sodium [29], where the internal degrees of freedom of spin were activated by the optical dipole potential trap, there followed a vast of physical experiments of various spinor BEC [24, 31] and theoretically investigations to explore various peculiar quantum phenomena [25]. In spinor BEC, particles of different hyperfine states allow for different angular momentum spaces, leading to very rich spin structures. Therefore, degenerate spinor quantum gases simultaneously exhibit magnetic

*Corresponding author
Email addresses: liyu@tjufe.edu.cn (Yu LI), zhixuan_li@stu.scu.edu.cn (Zhixuan LI), mtxie@tju.edu.cn (Manting XIE), Zhang_Yong@tju.edu.cn (Yong ZHANG)

and superfluid properties and shed light on a wide range of topics such as topological quantum structures, fractional quantum Hall effects, etc [20, 30].

At temperature T much smaller than the critical condensate temperature T_c [5], a spin-1 BEC is well described by the three-component wave function $\Psi(\boldsymbol{x}, t) = (\psi_1(\boldsymbol{x}, t), \psi_0(\boldsymbol{x}, t), \psi_{-1}(\boldsymbol{x}, t))^\top$, whose evolution is governed by the coupled Gross-Pitaevskii equations (GPEs) [15, 30, 37]. In dimensionless form, the d-dimensional ($d = 1, 2,$ or 3) GPEs could be unified as [5, 6]

$$i\partial_t \psi_1 = \left[-\frac{1}{2}\nabla^2 + V(\boldsymbol{x}) + \beta_n \rho + \beta_s \left(|\psi_0|^2 + \rho_z \right) \right] \psi_1 + \beta_s \psi_0^2 \bar{\psi}_{-1}, \tag{1.1a}$$

$$i\partial_t \psi_0 = \left[-\frac{1}{2}\nabla^2 + V(\boldsymbol{x}) + \beta_n \rho + \beta_s \left(|\psi_1|^2 + |\psi_{-1}|^2 \right) \right] \psi_0 + 2\beta_s \psi_1 \bar{\psi}_0 \psi_{-1}, \tag{1.1b}$$

$$i\partial_t \psi_{-1} = \left[-\frac{1}{2}\nabla^2 + V(\boldsymbol{x}) + \beta_n \rho + \beta_s \left(|\psi_0|^2 - \rho_z \right) \right] \psi_{-1} + \beta_s \bar{\psi}_1 \psi_0^2, \tag{1.1c}$$

where t denotes time and $\boldsymbol{x} = x \in \mathbb{R}$, $\boldsymbol{x} = (x, y)^\top \in \mathbb{R}^2$ and/or $\boldsymbol{x} = (x, y, z)^\top \in \mathbb{R}^3$ is the Cartesian coordinate vector, $\rho = \sum_{j=-1}^{1} |\psi_j|^2$ is the density function and $\rho_z = |\psi_1|^2 - |\psi_{-1}|^2$. $V(\boldsymbol{x})$ is a real-valued external potential that is case-dependent and one common choice is the following harmonic trapping potential

$$V(\boldsymbol{x}) = \frac{1}{2} \begin{cases} \gamma_x^2 x^2, & d = 1, \\ \gamma_x^2 x^2 + \gamma_y^2 y^2, & d = 2, \\ \gamma_x^2 x^2 + \gamma_y^2 y^2 + \gamma_z^2 z^2, & d = 3. \end{cases} \tag{1.2}$$

Here, $\gamma_\alpha > 0$ ($\alpha = x, y, z$) are dimensionless constants proportional to the trapping frequency in the α-direction. Constant β_n denotes the mean-field interaction, and β_s represents spin-exchange interaction with positive/negative β_s corresponding to the anti-ferromagnetic/ferromagnetic case.

Introduce the triple of spin-1 Pauli matrices $\mathbf{S} = (\mathbf{S}_x, \mathbf{S}_y, \mathbf{S}_z)$ as

$$\mathbf{S}_x = \frac{1}{\sqrt{2}} \begin{bmatrix} 0 & 1 & 0 \\ 1 & 0 & 1 \\ 0 & 1 & 0 \end{bmatrix}, \quad \mathbf{S}_y = \frac{i}{\sqrt{2}} \begin{bmatrix} 0 & -1 & 0 \\ 1 & 0 & -1 \\ 0 & 1 & 0 \end{bmatrix}, \quad \mathbf{S}_z = \begin{bmatrix} 1 & 0 & 0 \\ 0 & 0 & 0 \\ 0 & 0 & -1 \end{bmatrix},$$

and the spin vector

$$\mathbf{s}(\Psi) = (\mathbf{s}_x(\Psi), \mathbf{s}_y(\Psi), \mathbf{s}_z(\Psi))^\top = (\Psi^\mathsf{H} \mathbf{S}_x \Psi, \Psi^\mathsf{H} \mathbf{S}_y \Psi, \Psi^\mathsf{H} \mathbf{S}_z \Psi)^\top,$$

where $\bar{\boldsymbol{\zeta}}$, $\boldsymbol{\zeta}^\mathsf{H} := (\bar{\boldsymbol{\zeta}})^\top$ are conjugate and conjugate transpose of vector $\boldsymbol{\zeta} \in \mathbb{C}^{3 \times 1}$ respectively. Note that Pauli matrices are all Hermitian, i.e., $\mathbf{S}_j^\mathsf{H} = \mathbf{S}_j$ for $j = x, y, z$. The GPEs (1.1) can be written in a compact form

$$i\partial_t \Psi = \left((L + \beta_n \rho) \mathbf{I}_3 + \beta_s \, \mathbf{S} \cdot \mathbf{s}(\Psi) \right) \Psi, \tag{1.3}$$

where $L = -\frac{1}{2}\nabla^2 + V(\boldsymbol{x})$, $\mathbf{I}_3$ is identity matrix, and

$$\mathbf{S} \cdot \mathbf{s}(\Psi) \quad := \quad \mathbf{S}_x \, \mathbf{s}_x(\Psi) + \mathbf{S}_y \, \mathbf{s}_y(\Psi) + \mathbf{S}_z \, \mathbf{s}_z(\Psi).$$

The GPEs (1.1) conserves three important quantities: the *mass*

$$\mathcal{N}(\Psi(\cdot, t)) = \|\Psi(\cdot, t)\|^2 := \int_{\mathbb{R}^d} \sum_{j=-1}^{1} |\psi_j(\boldsymbol{x})|^2 \, \mathrm{d}\boldsymbol{x} \equiv \mathcal{N}(\Psi(\cdot, 0)) = 1, \qquad t \geq 0,$$

2

the *magnetization* (with $-1 \leq M \leq 1$)

$$\mathcal{M}(\Psi(\cdot, t)) := \int_{\mathbb{R}^d} \left(|\psi_1(\boldsymbol{x})|^2 - |\psi_{-1}(\boldsymbol{x})|^2 \right) \mathrm{d}\boldsymbol{x} \equiv \mathcal{M}(\Psi(\cdot, 0)) = M, \qquad t \geq 0,$$

and *energy*

$$
\begin{aligned}
\mathcal{E}(\Psi(\cdot, t)) \ &:= \ \int_{\mathbb{R}^d} \left\{ \sum_{j=-1}^{1} \left(\frac{1}{2} |\nabla \psi_j(\boldsymbol{x})|^2 + V(\boldsymbol{x})|\psi_j(\boldsymbol{x})|^2 \right) + \frac{\beta_n}{2} |\Psi(\boldsymbol{x})|^4 + \frac{\beta_s}{2} |\mathbf{s}(\Psi(\boldsymbol{x}))|^2 \right\} \mathrm{d}\boldsymbol{x} \\
&\equiv \ \mathcal{E}(\Psi(\cdot, 0)), \quad t \geq 0,
\end{aligned}
$$

where $|\Psi|$ is length of vector Ψ, that is, $|\Psi| := \sqrt{|\psi_1|^2 + |\psi_0|^2 + |\psi_{-1}|^2} = \sqrt{\rho}$. The ground state, denoted by $\Phi_g = (\phi_1^g, \phi_0^g, \phi_{-1}^g)^\top$, is defined as minimizer of the following problem

$$\Phi_g = \arg \min_{\Phi \in \mathcal{S}_M} \mathcal{E}(\Phi), \tag{1.4}$$

where $\mathcal{S}_M$ is the constraint functional space

$$\mathcal{S}_M := \left\{ \Phi = (\phi_1, \phi_0, \phi_{-1})^\top \mid \|\Phi\|^2 = 1, \ \|\phi_1\|^2 - \|\phi_{-1}\|^2 = M, \ \mathcal{E}(\Phi) < \infty \right\}.$$

The ground state Φ_g satisfies the following Euler-Lagrange equations

$$\Lambda \Phi = \mathbf{H} \Phi := \left(\left(L + \beta_n \rho \right) \mathbf{I}_3 + \beta_s \, \mathbf{S} \cdot \mathbf{s}(\Phi) \right) \Phi, \tag{1.5}$$

where $\mathbf{H} = \mathrm{diag}(H_1, H_0, H_{-1})$ is the Hamiltonian operators, $\Phi = (\phi_1, \phi_0, \phi_{-1})^\top$, $\Lambda = \mathrm{diag}(\mu_1, \mu_0, \mu_{-1})$ with entry μ_j, given below as the chemical potential associated with the j-th component [5, 6],

$$\mu_j = \frac{\int_{\mathbb{R}^d} \overline{\phi_j} H_j \phi_j \mathrm{d}\boldsymbol{x}}{\int_{\mathbb{R}^d} |\phi_j|^2 \mathrm{d}\boldsymbol{x}}, \quad j = 1, 0, -1, \tag{1.6}$$

satisfying relation $\mu_1 + \mu_{-1} = 2\mu_0$. We can construct stationary states of (1.1) in the following way

$$\Psi_s(\boldsymbol{x}, t) = \mathrm{diag}(e^{-\mathrm{i}\mu_1 t}, e^{-\mathrm{i}\mu_0 t}, e^{-\mathrm{i}\mu_{-1} t}) \Phi_s(\boldsymbol{x}), \tag{1.7}$$

where $\Phi_s = (\phi_1^s, \phi_0^s, \phi_{-1}^s)^\top$ and $\{\mu_1, \mu_0, \mu_{-1}\}$ are solutions to the nonlinear eigenvalue problem (1.5).

On the mean-field level, the many-body effects are absent and the GPE (1.1) proves to be valid for the spin-1 BEC [15, 30, 37]. However, due to the many-body effect of interatomic interactions, there are excitations in the system even in the lowest energy state, which could be regarded as quasi-particles and are known as elementary/collective excitations [7]. We first need to go beyond the mean-field theory to study elementary/collective excitations. Under the proper assumption, the elementary/collective excitation around the mean-field stationary state could be well described within the Bogoliubov theory, which resulted in the celebrated Bogoliubov-de Gennes (BdG) equations [4, 11, 13, 17]. As elementary/collective excitation of BEC provides fundamental information about the ultracold quantum state, different phases of a trapped spin-1 BEC feature distinctive elementary/collective excitations, therefore, they could be used to distinguish various phases.

3

The first experimental measurements of the lowest elementary/collective modes of BECs were performed in [19]. Since then, great enthusiasm has been stimulated to mathematical and numerical investigation of BdG equations in the past few decades [16, 32]. Along the numerical front, there are many successful researches devoted to BdG corresponding to various BECs based on the well-known ARPACK library, and we refer to [10, 11, 12, 33] for an incomplete list. The spatial discretization of the wavefunction, eigenfunction, and linear differential operators can be categorized into finite difference method [12, 13], finite-element method [10, 26] and Fourier/sine spectral method [33, 38]. For low dimension problem ($d = 1, 2$), the resulting eigensystem is solved with either direct eigensolver, e.g., using "eigs" with MATLAB or iterative subspace solver, such as ARPACK or the locally optimal block preconditioned 4-d conjugate gradient [2, 3].

Up to now, there have been relatively few theoretical studies on the excitation of spin-1 BEC. Most numerical studies have focused on lower-dimensional cases ($d = 1$ or 2), for example, the low-lying elementary/collective excitations of quasi-two-dimensional rotating systems [11, 38] and cylindrically symmetric systems [36]. Chen *et al.* [9] directly solved the BdG equations for spin-orbit BEC using the Arnoldi method, while the Arnoldi method with ARPACK was adapted to study the dipolar spin-1 BEC [11]. Recently, Tang *et al.* [33, 38] construct efficient and spectral numerical algorithms for the BdG equations of dipolar BEC in higher-dimensional spaces.

As far as we know, there have been quite few mathematical or numerical studies on the BdG excitations of spin-1 BEC. Hence, it is necessary to develop mathematical theories and construct an accurate and efficient eigensolver. To numerically study the elementary/collective excitations, there are two main challenges: (i) an accurate stationary state solver, especially the ground state solver; (ii) an accurate and efficient BdG solver. As for the computation of ground state, various numerical methods have been proposed for the spin-1 BEC, such as the gradient flow method [5, 6], the gradient flow with the Lagrange multiplier (GFLM) method [22],and regularized Newton method [35] etc. Here, we adopt GFLM to compute the ground state due to its simplicity and effectiveness.

As is known, the structure of eigenvalue distribution and the generalized nullspace is of essential importance to eigensolver performance in terms of efficiency, accuracy and stability. It is noted that eigenvalues, coming in negative/positive pairs, are real and span over the real line to infinity, and the eigenspace corresponding to eigenvalues of different magnitudes are bi-orthogonal [21]. More importantly, for eigenvalue zero, the algebraic multiplicity may not be equal to its geometric multiplicity, thus leading to a rich and complex generalized nullspace structure. However, such peculiar inherent structure and analytical properties have not been considered or taken into account in the state-of-art popular solvers, for example, the ARPACK library is much more a general-purpose eigensolver. Direct application of the aforementioned solvers may encounter slow convergence or even divergence, especially at eigenvalue zero, and the performance will definitely deteriorate in high-dimension problems.

To make it more challenging, the eigenfunctions are usually discretized by the Fourier spectral method, therefore, the resulted discrete eigensystem is a fully-populated dense matrix, which renders prohibitively huge memory costs if one chooses to store the matrix explicitly. Therefore, it is imperative to adopt some iterative algorithm, where one only needs to provide a matrix-vector product or operator-function evaluation, so to bypass the huge explicit matrix storage, and gain good parallel scalability for large-scale high dimension problems.

Overall, the main contributions of this paper are fourfold:

1. derive the BdG equations for spin-1 Bose-Einstein condensates around the ground state and investigate its mathematical structures, including analytical eigenvalues/eigenfunctions, generalized nullspace, and the bi-orthogonality between eigenspaces;

2. develop a bi-orthogonal structure-preserving Fourier spectral eigensolver, and propose an efficient implementation of the matrix-vector product based on the Fourier spectral method;

3. prove the numerical stability and spectral convergence;

4. verify its spectral accuracy, efficiency, and scalability, and numerically study the excitation spectrum and Bogoliubov amplitudes around the ground state with different parameters in 1D, 2D, and 3D.

The rest of the paper is organized as follows: In Section 2, we introduce the BdG equations and derive some analytical properties. In Section 3, we present details of the Fourier spectral method for space discretization and propose an efficient eigensolver. Extensive numerical examples are shown in Section 4 to confirm the performance of our method, together with some applications to study the solutions to the BdG equations with different parameters in 1D, 2D, and 3D. Finally, conclusions are drawn in Section 5.

2. The BdG equations and its properties

2.1. The Bogoliubov-de Gennes equations

To characterize the elementary/collective excitations of a spin-1 BEC, the Bogoliubov theory [4, 11] begins with the ground state Φ_g of the CGPEs (1.3), which are also the solution of the nonlinear eigenvalue problems (1.5) with corresponding chemical potentials μ_1, μ_0 and μ_{-1}, and assumes the evolution of CGPEs (1.3) is around Φ_g. The corresponding wave function Ψ takes the following form [18, 33]

$$\Psi(\boldsymbol{x}, t) = \mathrm{diag}\big(e^{-\mathrm{i}\mu_1 t}, e^{-\mathrm{i}\mu_0 t}, e^{-\mathrm{i}\mu_{-1} t}\big) \left[\Phi_g(\boldsymbol{x}) + \varepsilon \sum_{\ell=1}^{\infty} \Big(\boldsymbol{u}^\ell(\boldsymbol{x}) e^{-\mathrm{i}\omega_\ell t} + \bar{\boldsymbol{v}}^\ell(\boldsymbol{x}) e^{\mathrm{i}\omega_\ell t}\Big)\right], \qquad (2.1)$$

for $\boldsymbol{x} \in \mathbb{R}^d$ and $t > 0$. Here, $0 < \varepsilon \ll 1$ is a small quantity used to control the population of quasiparticle excitation, $\omega_\ell \in \mathbb{C}$ is the frequency of the excitations to be determined, and $\boldsymbol{u}^\ell, \boldsymbol{v}^\ell \in H^1(\mathbb{R}^3; \mathbb{C}^3)$ are the Bogoliubov excitation modes satisfying normalization condition

$$\int_{\mathbb{R}^d} \Big(|\boldsymbol{u}^\ell(\boldsymbol{x})|^2 - |\boldsymbol{v}^\ell(\boldsymbol{x})|^2\Big) \,\mathrm{d}\boldsymbol{x} = \int_{\mathbb{R}^d} \sum_{j=-1}^{1} \Big(|u_j^\ell(\boldsymbol{x})|^2 - |v_j^\ell(\boldsymbol{x})|^2\Big) \,\mathrm{d}\boldsymbol{x} = 1, \quad \ell \in \mathbb{Z}^+. \qquad (2.2)$$

where $\boldsymbol{u}^\ell = (u_1^\ell, u_0^\ell, u_{-1}^\ell)^\top$, $\boldsymbol{v}^\ell = (v_1^\ell, v_0^\ell, v_{-1}^\ell)^\top$. Plugging (2.1) into (1.3), by collecting linear terms in ε and separating frequency $e^{-i\omega_\ell t}$ and $e^{i\omega_\ell t}$, we obtain the BdG equations as follows

$$\begin{bmatrix} \mathcal{A} & \mathcal{B} \\ -\mathcal{C} & -\mathcal{D} \end{bmatrix} \begin{bmatrix} \boldsymbol{u} \\ \boldsymbol{v} \end{bmatrix} = \omega \begin{bmatrix} \boldsymbol{u} \\ \boldsymbol{v} \end{bmatrix}, \qquad (2.3)$$

with constraint

$$\int_{\mathbb{R}^d} \big(|\boldsymbol{u}(\boldsymbol{x})|^2 - |\boldsymbol{v}(\boldsymbol{x})|^2\big) \,\mathrm{d}\boldsymbol{x} = 1, \qquad (2.4)$$

5

where all the subscripts ℓ are omitted hereafter for simplicity, ω is the excitation energy and the operators are given explicitly

$$\mathcal{A} = (L\mathbf{I}_3 - \Lambda) + \beta_n\big(\rho\mathbf{I}_3 + \Phi_g\Phi_g^{\mathsf{H}}\big) + \beta_s\bigg(\mathbf{S}\cdot\mathbf{s}(\Phi_g) + \sum_{j=x,y,z}\mathbf{S}_j\Phi_g\Phi_g^{\mathsf{H}}\mathbf{S}_j^{\mathsf{H}}\bigg), \tag{2.5}$$

$$\mathcal{B} = \beta_n\Phi_g\Phi_g^{\top} + \beta_s\sum_{j=x,y,z}\mathbf{S}_j\Phi_g\Phi_g^{\top}\mathbf{S}_j^{\top}, \tag{2.6}$$

$$\mathcal{C} = \beta_n\bar{\Phi}_g\Phi_g^{\mathsf{H}} + \beta_s\sum_{j=x,y,z}\bar{\mathbf{S}}_j\bar{\Phi}_g\Phi_g^{\mathsf{H}}\mathbf{S}_j^{\mathsf{H}}, \tag{2.7}$$

$$\mathcal{D} = (L\mathbf{I}_3 - \Lambda) + \beta_n\big(\rho\mathbf{I}_3 + \bar{\Phi}_g\Phi_g^{\top}\big) + \beta_s\bigg(\bar{\mathbf{S}}\cdot\mathbf{s}(\Phi_g) + \sum_{j=x,y,z}\bar{\mathbf{S}}_j\bar{\Phi}_g\Phi_g^{\top}\mathbf{S}_j^{\top}\bigg). \tag{2.8}$$

It is easy to check that $\mathcal{A}$ and $\mathcal{D}$ are both Hermitian operators, i.e., $\mathcal{A}^* = \mathcal{A}$, $\mathcal{D}^* = \mathcal{D}$, and $\mathcal{B}^* = \mathcal{C}$, where symbol $*$ denotes the operator adjoint associated with inner product $\langle\boldsymbol{f},\boldsymbol{g}\rangle := \sum_{j=-1}^{1}\int_{\mathbb{R}^d}f_j(\boldsymbol{x})\overline{g_j(\boldsymbol{x})}\,\mathrm{d}\boldsymbol{x}$. Furthermore, we have $\overline{\mathcal{A}\boldsymbol{g}} = \mathcal{D}\bar{\boldsymbol{g}}$, $\overline{\mathcal{B}\boldsymbol{g}} = \mathcal{C}\bar{\boldsymbol{g}}$, $\forall\,\boldsymbol{g}\in H^1(\mathbb{R}^d;\mathbb{C}^3)$, and it immediately implies the operators's finite-dimension subspace representations, denoted by matrices A, B, C and D, are either Hermitian or symmetric, that is,

$$A^{\mathsf{H}} = A, \quad D = \overline{A}, \quad B^{\top} = B \quad \text{and} \quad C = \overline{B}. \tag{2.9}$$

The matrices representation of (2.3) reads as follows

$$\begin{bmatrix} A & B \\ -\overline{B} & -\overline{A} \end{bmatrix}\begin{bmatrix} \mathbf{u} \\ \mathbf{v} \end{bmatrix} = \omega\begin{bmatrix} \mathbf{u} \\ \mathbf{v} \end{bmatrix}, \tag{2.10}$$

and it coincides with the Bethe-Salpeter Hamiltonian (BSH) matrix arising from optical absorption spectrum analysis [27].

2.2. Analytical properties

In this section, we derive some analytical properties of the BdG equations as well as the structure of generalized nullspace for both ferromagnetic and anti-ferromagnetic cases. They might serve as benchmarks for numerical solutions or help to design an efficient eigensolver.

Theorem 2.1 (Symmetric distribution). *If $\{\omega;\boldsymbol{u},\boldsymbol{v}\}$ is a solution pair to the BdG equations (2.3), then $\{-\bar{\omega};\bar{\boldsymbol{v}},\bar{\boldsymbol{u}}\}$ is also a solution pair. Furthermore, If $(\boldsymbol{u},\boldsymbol{v})$ satisfies the normalization constraint (2.4), i.e., the elementary/collective excitations, the frequency ω is real.*

Proof. The first conclusion can be proved by taking the conjugate of Eqn. (2.3). Multiplying the first/second equation of (2.3) by $\boldsymbol{u}/\boldsymbol{v}$ respectively and integrating each equation concerning $\boldsymbol{x}$, we subtract the second integration from the first one to obtain the following

$$\langle\boldsymbol{u},\mathcal{A}\boldsymbol{u}\rangle + \langle\boldsymbol{u},\mathcal{B}\boldsymbol{v}\rangle + \langle\boldsymbol{v},\mathcal{C}\boldsymbol{u}\rangle + \langle\boldsymbol{v},\mathcal{D}\boldsymbol{v}\rangle = \bar{\omega}\int_{\mathbb{R}^d}(|\boldsymbol{u}(\boldsymbol{x})|^2 - |\boldsymbol{v}(\boldsymbol{x})|^2)\,\mathrm{d}\boldsymbol{x}. \tag{2.11}$$

From Eqn. (2.4), we can see that ω is real.

$\square$

As shown in [5], under appropriate assumptions, the ground states can be chosen as real-valued functions. Therefore, in this article, we shall focus on the real ground state hereafter, and all operators involved are real. To be more specific,

$$\mathcal{D} = \mathcal{A}, \quad \mathcal{C} = \mathcal{B}.$$

The BdG equation (2.3) is a linear response eigenvalue problem of the following form

$$\begin{bmatrix} \mathcal{A} & \mathcal{B} \\ -\mathcal{B} & -\mathcal{A} \end{bmatrix} \begin{bmatrix} \boldsymbol{u} \\ \boldsymbol{v} \end{bmatrix} = \omega \begin{bmatrix} \boldsymbol{u} \\ \boldsymbol{v} \end{bmatrix}. \tag{2.12}$$

By applying a change of variables

$$\boldsymbol{u} = \boldsymbol{f} + \boldsymbol{g}, \ \boldsymbol{v} = \boldsymbol{f} - \boldsymbol{g}, \tag{2.13}$$

the above equation can be reformulated

$$\mathcal{H} \begin{bmatrix} \boldsymbol{f} \\ \boldsymbol{g} \end{bmatrix} := \begin{bmatrix} \mathcal{O} & \mathcal{H}_- \\ \mathcal{H}_+ & \mathcal{O} \end{bmatrix} \begin{bmatrix} \boldsymbol{f} \\ \boldsymbol{g} \end{bmatrix} = \omega \begin{bmatrix} \boldsymbol{f} \\ \boldsymbol{g} \end{bmatrix}, \tag{2.14}$$

where $\mathcal{H}_- := \mathcal{A} - \mathcal{B}$ and $\mathcal{H}_+ := \mathcal{A} + \mathcal{B}$ are both Hermitian operators, and the constraint (2.4) is reformulated in $(\boldsymbol{f}, \boldsymbol{g})$ as

$$\langle \boldsymbol{f}, \boldsymbol{g} \rangle = \frac{1}{4}. \tag{2.15}$$

Remark 2.1. *If $\mathcal{H}_+$ is positive definite, according to Lemma 2.3 of [21], the constrain (2.4) implies that the eigenvalue ω is nonzero, therefore, we shall only focus on the* **non-zero** *eigenvalues and their eigenfunctions.*

Theorem 2.2 (**Analytical eigenparis**)**.** *Let $\Phi_g = (\phi_1^g, \phi_0^g, \phi_{-1}^g)^\top$ be real-valued ground states for Eqn. (1.1) with harmonic trapping potential (1.2), we have analytical solutions to BdG equation (2.3) as follows*

$$\{\omega_\alpha; \boldsymbol{u}_\alpha, \boldsymbol{v}_\alpha\} := \left\{ \gamma_\alpha; \frac{1}{\sqrt{2}} \left(\gamma_\alpha^{-\frac{1}{2}} \partial_\alpha \Phi_g - \gamma_\alpha^{\frac{1}{2}} \alpha \Phi_g \right), \frac{1}{\sqrt{2}} \left(\gamma_\alpha^{-\frac{1}{2}} \partial_\alpha \Phi_g + \gamma_\alpha^{\frac{1}{2}} \alpha \Phi_g \right) \right\}, \tag{2.16}$$

with $\alpha = x$ in one dimension, $\alpha = x, y$ in two dimensions and $\alpha = x, y, z$ in three dimensions.

Proof. For simplicity, we only prove the $\alpha = x$ case and extensions to other spatial variables are similar. Differentiate (1.5) with respect to x and combine $\mathcal{H}_+$ definition, we derive

$$\mathcal{H}_+(\partial_x \Phi_g) = \gamma_x(-\gamma_x x \Phi_g),$$

with $\partial_x \Phi_g = (\partial_x \phi_1^g, \partial_x \phi_0^g, \partial_x \phi_{-1}^g)^\top$. Apply $\mathcal{H}_-$ on $-\gamma_x x \Phi_g$, we have

$$\mathcal{H}_-(-\gamma_x x \Phi_g) = \gamma_x(\partial_x \Phi_g).$$

Therefore, we can see that $(\partial_x \Phi_g^\top, -\gamma_x x \Phi_g^\top)^\top$ solves (2.14) with $\omega = \gamma_x$. With simple calculations, we have

$$\langle -\gamma_x x \Phi_g, \partial_x \Phi_g \rangle = \int_{\mathbb{R}^2} \sum_{j=-1}^{1} \left(-\gamma_x x \phi_j^g \partial_x \phi_j^g \right) \mathrm{d}x \mathrm{d}y = \frac{\gamma_x}{2}.$$

Therefore, the normalized function $(\boldsymbol{f}, \boldsymbol{g}) = \left(\frac{1}{\sqrt{2}} \gamma_x^{-\frac{1}{2}} \partial_x \Phi_g, -\frac{1}{\sqrt{2}} \gamma_x^{\frac{1}{2}} x \Phi_g \right)$ solves (2.14) with eigenvalue $\omega = \gamma_x$. Finally, we derive the following analytic solutions

$$\omega_x = \gamma_x, \quad \boldsymbol{u}_x = \frac{1}{\sqrt{2}} \left(\gamma_x^{-\frac{1}{2}} \partial_x \Phi_g - \gamma_x^{\frac{1}{2}} x \Phi_g \right), \quad \boldsymbol{v}_x = \frac{1}{\sqrt{2}} \left(\gamma_x^{-\frac{1}{2}} \partial_x \Phi_g + \gamma_x^{\frac{1}{2}} x \Phi_g \right).$$

$\square$

Theorem 2.3 (Biorthogonality). *Assume $\{\omega_i; \boldsymbol{f}_i, \boldsymbol{g}_i\}_{i=1}^2$ are eigenpairs of Eqn. (2.14) with eigenvalues of different magnitudes, i.e., $|\omega_1| \neq |\omega_2|$, the following biorthogonal properties hold true*

$$\langle \boldsymbol{f}_1, \boldsymbol{g}_2 \rangle = \langle \boldsymbol{f}_2, \boldsymbol{g}_1 \rangle = 0.$$

Proof. Using Eqn. (2.14), we have

$$\omega_i^2 \langle \boldsymbol{f}_i, \boldsymbol{g}_j \rangle = \langle \mathcal{H}_- \mathcal{H}_+ \boldsymbol{f}_i, \boldsymbol{g}_j \rangle = \langle \boldsymbol{f}_i, \mathcal{H}_+ \mathcal{H}_- \boldsymbol{g}_j \rangle = \omega_j^2 \langle \boldsymbol{f}_i, \boldsymbol{g}_j \rangle,$$

which means

$$(\omega_i^2 - \omega_j^2) \langle \boldsymbol{f}_i, \boldsymbol{g}_j \rangle = 0.$$

Since $|\omega_i| \neq |\omega_j|$, we obtain $\langle \boldsymbol{f}_i, \boldsymbol{g}_j \rangle = 0, \quad \text{for } i \neq j.$ $\square$

2.3. Generalized nullspace

As is known, the algebraic/geometric multiplicity of eigenvalue zero and the structure of its associated generalized nullspace are of great importance to the eigensolver's performance in terms of convergence, accuracy and efficiency. The generalized nullspace of $\mathcal{H}$ is defined as nullspace of $\mathcal{H}^p$ for some positive integer p such that

$$\mathrm{null}(\mathcal{H}^p) = \mathrm{null}(\mathcal{H}^{p+1}).$$

For compact operator $\mathcal{H}$, the integer p is finite and $\mathrm{null}(\mathcal{H}^p) = \mathrm{null}(\mathcal{H}^q)$ holds true for any greater integer q, i.e, $q \geq p$. In this subsection, we shall elaborate on the structure of generalized nullspace for ferromagnetic and antiferromagnetic systems, which is of course closely connected with the nullspace of $\mathcal{H}_-$ and $\mathcal{H}_+$.

Case I: Ferromagnetic system ($\beta_s < 0$).

For the ferromagnetic system, when the following conditions hold, i.e.,

$$M \in (-1, 1), \ \beta_s < 0, \ \text{and} \ \beta_n + \beta_s \geq 0, \tag{2.17}$$

we have the single mode approximation, i.e. each component of the ground state Φ_g is identical up to a constant factor, which is given in Lemma 2.1.

Lemma 2.1 (Single Mode approximation (SMA) [5, Theorem 4.2]). *Under conditions (2.17), there exists a ground state solution $\Phi_g = \boldsymbol{a} \phi_g$, $\boldsymbol{a} = \left(\frac{1+M}{2}, \left(\frac{1-M^2}{2} \right)^{1/2}, \frac{1-M}{2} \right)^\top$, and the chemical potentials are identical, i.e., $\mu_1 = \mu_0 = \mu_{-1}$. Here, ϕ_g is the unique positive minimizer of the following energy functional*

$$E_{SMA}(\phi) = \int_{\mathbb{R}^d} \left[\frac{1}{2} |\nabla \phi|^2 + V(\boldsymbol{x}) |\phi|^2 + \frac{\beta_n + \beta_s}{2} |\phi|^4 \right] \mathrm{d}\boldsymbol{x},$$

under constraint $\mathcal{S} := \left\{ \phi \in L^2(\mathbb{R}^d) \big| \|\phi\|^2 = 1, E_{SMA}(\phi) < \infty \right\}.$

8

Theorem 2.4 (Nullspace of $\mathcal{H}_-$ and $\mathcal{H}_+$ for ferromagnetic system). *Under conditions* (2.17), *we derive the nullspace of* $\mathcal{H}_-$ *and* $\mathcal{H}_+$ *as follows*

$$\mathrm{null}(\mathcal{H}_-) = \mathrm{span}\{\Phi_1, \Phi_2\}, \qquad \mathrm{null}(\mathcal{H}_+) = \mathrm{span}\{\Phi_2\}, \tag{2.18}$$

where $\Phi_1 = \Phi_g = \boldsymbol{a}\,\phi_g$, $\Phi_2 = \boldsymbol{b}\,\phi_g$ *with* $\boldsymbol{b} = \left((\frac{1-M^2}{2})^{1/2}, -M, -(\frac{1-M^2}{2})^{1/2}\right)^\top$.

Moreover, $\mathcal{H}_-$ *and* $\mathcal{H}_+$ *are positive semidefinite.*

Proof. It is straightforward to check that

$$\mathcal{H}_- = \mathcal{A} - \mathcal{B} = \left(L + (\beta_n + \beta_s)\phi_g^2 - \mu\right)\mathbf{I}_3 + \beta_s\phi_g^2\left(\mathbf{S}\cdot\mathbf{s}(\boldsymbol{a}) + \mathbf{S}_y\boldsymbol{a}\boldsymbol{a}^\top\mathbf{S}_y^{\mathsf{H}} - \mathbf{S}_y\boldsymbol{a}\boldsymbol{a}^\top\mathbf{S}_y^\top - \mathbf{I}_3\right),$$

where $\mu = \mu_1 = \mu_0 = \mu_{-1}$ in Lemma 2.1. Moreover, we have

$$\mathcal{W}^{-1}\left(\mathbf{S}\cdot\mathbf{s}(\boldsymbol{a}) + \mathbf{S}_y\boldsymbol{a}\boldsymbol{a}^\top\mathbf{S}_y^{\mathsf{H}} - \mathbf{S}_y\boldsymbol{a}\boldsymbol{a}^\top\mathbf{S}_y^\top - \mathbf{I}_3\right)\mathcal{W} = \begin{bmatrix} 0 & 0 & 0 \\ 0 & 0 & 0 \\ 0 & 0 & -2 \end{bmatrix},$$

where $\mathcal{W} = [\boldsymbol{a}, \boldsymbol{b}, \boldsymbol{c}]$ is an orthogonal symmetric matrix with the third column $\boldsymbol{c} = \left(\frac{1-M}{2}, -(\frac{1-M^2}{2})^{1/2}, \frac{1+M}{2}\right)^\top$. Then, we can diagonalize operator $\mathcal{H}_-$ using $\mathcal{W}$ as $\mathcal{W}^{-1}\mathcal{H}_-\mathcal{W} = \mathcal{K}$, where $\mathcal{K}$ reads explicitly as follows

$$\mathcal{K} = \mathrm{diag}\left(L + (\beta_n + \beta_s)\phi_g^2 - \mu, L + (\beta_n + \beta_s)\phi_g^2 - \mu, L + (\beta_n - \beta_s)\phi_g^2 - \mu\right).$$

According to Lemmas 1 & 2 in [8], $\mathrm{null}\left(L + (\beta_n + \beta_s)\phi_g^2 - \mu\right) = \mathrm{span}\{\phi_g\}$, and $L + (\beta_n - \beta_s)\phi_g^2 - \mu$ is symmetric positive definite. Hence, we can derive nullspace of $\mathcal{K}$ as

$$\mathrm{null}(\mathcal{K}) = \mathrm{span}\left\{\begin{bmatrix} 1 \\ 0 \\ 0 \end{bmatrix}\phi_g, \begin{bmatrix} 0 \\ 1 \\ 0 \end{bmatrix}\phi_g\right\}.$$

Therefore, we obtain

$$\mathrm{null}(\mathcal{H}_-) = \mathrm{span}\{\Phi_1, \Phi_2\} = \mathrm{span}\{\boldsymbol{a}\,\phi_g, \boldsymbol{b}\,\phi_g\}.$$

Similarly, we have

$$\mathrm{null}(\mathcal{H}_+) = \mathrm{span}\{\Phi_2\}.$$

Proofs are similar and we choose to omit details for brevity. $\qquad\qquad\qquad\qquad\qquad\square$

Theorem 2.5 (Generalized nullspace of $\mathcal{H}$ for ferromagnetic system). *Under conditions* (2.17), *we have the nullspace of* $\mathcal{H}$ *as*

$$\mathrm{null}(\mathcal{H}) = \mathrm{span}\left\{\begin{bmatrix} \mathbf{0} \\ \Phi_1 \end{bmatrix}, \begin{bmatrix} \mathbf{0} \\ \Phi_2 \end{bmatrix}, \begin{bmatrix} \Phi_2 \\ \mathbf{0} \end{bmatrix}\right\}, \tag{2.19}$$

and the generalized nullspace

$$\mathrm{null}(\mathcal{H}^3) = \mathrm{null}(\mathcal{H}^2) = \mathrm{null}(\mathcal{H}) \oplus \mathrm{span}\left\{\begin{bmatrix} \widehat{\Phi}_1 \\ \mathbf{0} \end{bmatrix}\right\}, \tag{2.20}$$

where $\widehat{\Phi}_1$, *satisfying* $\mathcal{H}_+\widehat{\Phi}_1 = \Phi_1$, *is independent of* Φ_2.

9

Proof. For any $(\boldsymbol{f}^\top, \boldsymbol{g}^\top)^\top \in \mathrm{null}(\mathcal{H})$, we have $\boldsymbol{f} \in \mathrm{null}(\mathcal{H}_+)$ and $\boldsymbol{g} \in \mathrm{null}(\mathcal{H}_-)$. According to Theorem 2.4, we can prove Eqn. (2.19). Next, we shall investigate the nullspace of $\mathcal{H}^2$. For any $(\boldsymbol{f}^\top, \boldsymbol{g}^\top)^\top \in \mathrm{null}(\mathcal{H}^2)$, we have

$$\begin{bmatrix} \mathcal{O} & \mathcal{H}_- \\ \mathcal{H}_+ & \mathcal{O} \end{bmatrix} \begin{bmatrix} \boldsymbol{f} \\ \boldsymbol{g} \end{bmatrix} \in \mathrm{null}(\mathcal{H}). \tag{2.21}$$

It is worthy to note that Φ_2 does not belong to range of $\mathcal{H}_+$, i.e., $\Phi_2 \notin \mathcal{R}(\mathcal{H}_+)$. Otherwise, there exists a solution to $\mathcal{H}_+ \boldsymbol{f} = \Phi_2$, then we derive a contradiction

$$0 < \langle \Phi_2, \Phi_2 \rangle = \langle \Phi_2, \mathcal{H}_+ \boldsymbol{f} \rangle = \langle \mathcal{H}_+ \Phi_2, \boldsymbol{f} \rangle = 0.$$

Similarly, we can prove that $\Phi_2 \notin \mathcal{R}(\mathcal{H}_-)$. Therefore, equation (2.21) is equivalent to

$$\mathcal{H}_- \boldsymbol{g} = \mathbf{0}, \quad \mathcal{H}_+ \boldsymbol{f} = \Phi_1.$$

Since $\mathcal{H}_+$ is a self-adjoint compact operator, using the spectral theory of operator, the fact that $\Phi_1 \notin \mathrm{null}(\mathcal{H}_+)$ leads to $\Phi_1 \in \mathcal{R}(\mathcal{H}_+)$. That is, there exists a function $\widehat{\Phi}_1$ such that $\mathcal{H}_+ \widehat{\Phi}_1 = \Phi_1$. Then, we have

$$\mathrm{null}(\mathcal{H}^2) = \mathrm{null}(\mathcal{H}) \oplus \mathrm{span} \left\{ \begin{bmatrix} \widehat{\Phi}_1 \\ \mathbf{0} \end{bmatrix} \right\}.$$

Finally, we study the nullspace of $\mathcal{H}^3$. Similarly, if $\mathrm{null}(\mathcal{H}^2) \subsetneq \mathrm{null}(\mathcal{H}^3)$, we have the following equivalence

$$\begin{bmatrix} \mathcal{O} & \mathcal{H}_- \\ \mathcal{H}_+ & \mathcal{O} \end{bmatrix} \begin{bmatrix} \boldsymbol{f} \\ \boldsymbol{g} \end{bmatrix} = \begin{bmatrix} \widehat{\Phi}_1 \\ \mathbf{0} \end{bmatrix} \iff \begin{cases} \mathcal{H}_- \boldsymbol{g} = \widehat{\Phi}_1 \\ \mathcal{H}_+ \boldsymbol{f} = \mathbf{0} \end{cases}.$$

However, the above equation does not admit any solutions, and it can be proved using the following argument. If there exists a solution $\boldsymbol{g}$ satisfying $\mathcal{H}_- \boldsymbol{g} = \widehat{\Phi}_1$, then we have the following contradiction

$$0 = \langle \mathcal{H}_- \Phi_1, \boldsymbol{g} \rangle = \langle \Phi_1, \mathcal{H}_- \boldsymbol{g} \rangle = \langle \Phi_1, \widehat{\Phi}_1 \rangle = \langle \mathcal{H}_+ \widehat{\Phi}_1, \widehat{\Phi}_1 \rangle > 0.$$

That is to say, $\mathrm{null}(\mathcal{H}^3) = \mathrm{null}(\mathcal{H}^2)$, and proof is completed. $\qquad \square$

Case II: Anti-ferromagnetic system ($\beta_s > 0$).

For the anti-ferromagnetic system, when the following conditions hold, i.e.,

$$M \in (-1, 1), \ \beta_s > 0, \ \text{and} \ \beta_n \geq 0, \tag{2.22}$$

we have the vanishing phenomenon, i.e. the ground state $\Phi_g = (\phi_1^g, \phi_0^g, \phi_{-1}^g)^\top$ satisfies $\phi_0^g = 0$, which is presented in Lemma 2.2.

Lemma 2.2 ([5, Theorem 4.3]). *Under conditions* (2.22), *there exists a ground state solution* $\Phi_g = (\phi_1^g, 0, \phi_{-1}^g)^\top$ *and* (ϕ_1^g, ϕ_{-1}^g) *is a minimizer of the energy functional*

$$E_0(\phi_1, \phi_{-1}) = \int_{\mathbb{R}^d} \left[\sum_{j=\pm 1} \left(\frac{1}{2} |\nabla \phi_j|^2 + V(\boldsymbol{x}) |\phi_j|^2 \right) + \frac{\beta_n + \beta_s}{2} (|\phi_1|^4 + |\phi_{-1}|^4) + (\beta_n - \beta_s) |\phi_1|^2 |\phi_{-1}|^2 \right] \mathrm{d}\boldsymbol{x}$$

under constraint $\mathcal{S} := \left\{ (\phi_1, \ \phi_{-1}) \middle| \ \|\phi_1\|^2 = \frac{1+M}{2}, \ \|\phi_{-1}\|^2 = \frac{1-M}{2}, \ E_0(\phi_1, \phi_{-1}) < \infty \right\}.$

Theorem 2.6 (**Nullspace of $\mathcal{H}_-$ for anti-ferromagnetic system**). *Under conditions* (2.22), *we have the following property for nullspace of $\mathcal{H}_-$*

$$\text{span}\{\Phi_1, \Phi_2\} \subset \text{null}(\mathcal{H}_-),$$

where $\Phi_1 = \Phi_g$, $\Phi_2 = (b_1\phi_1^g, 0, b_{-1}\phi_{-1}^g)^\top$, and $(b_1, b_{-1}) = \left(-(\frac{1-M}{1+M})^{1/2}, (\frac{1+M}{1-M})^{1/2}\right)$.

Proof. Noticing the fact that $\phi_0 = 0$, we can reduce Eqn. (1.5) as follows

$$\begin{cases} [L - \mu_1 + \beta_n\rho + \beta_s(|\phi_1^g|^2 - |\phi_{-1}^g|^2)]\, \phi_1^g &= 0, \\ [L - \mu_{-1} + \beta_n\rho - \beta_s(|\phi_1^g|^2 - |\phi_{-1}^g|^2)]\, \phi_{-1}^g &= 0, \end{cases} \tag{2.23}$$

and the operator $\mathcal{H}_-$ is simplified below

$$\mathcal{H}_- = \text{diag}\Big(L - \mu_1 + \beta_n\rho + \beta_s\big(|\phi_1^g|^2 - |\phi_{-1}^g|^2\big), \quad L - \mu_0 + \beta_n\rho + \beta_s\big(\phi_1^g - \phi_{-1}^g\big)^2,$$
$$L - \mu_{-1} + \beta_n\rho - \beta_s\big(|\phi_1^g|^2 - |\phi_{-1}^g|^2\big)\Big).$$

Then, according to Eqn. (2.23), we obtain that Φ_1 and Φ_2 lie in the nullspace of $\mathcal{H}_-$, i.e., $\mathcal{H}_-\Phi_1 = 0$ and $\mathcal{H}_-\Phi_2 = 0$. It is easy to check that $\langle \Phi_1, \Phi_2 \rangle = 0$ and $\|\Phi_2\| = 1$ with $b_1 = -(\frac{1-M}{1+M})^{1/2}$, $b_{-1} = (\frac{1+M}{1-M})^{1/2}$. $\qquad\square$

Remark 2.2. *From our extensive numerical results not fully shown here, we conjecture that the following property holds for anti-ferromagnetic systems, that is,*

$$\mathcal{H}_+ \text{ is invertible} \qquad and \qquad \text{null}(\mathcal{H}_-) = \text{span}\{\Phi_1, \Phi_2\}.$$

Moreover, $\mathcal{H}_+$ is positive definite. and $\mathcal{H}_-$ is positive semidefinite.

If the above property is true, we can obtain the generalized nullspace of $\mathcal{H}$ as follows

$$\text{null}(\mathcal{H}^3) = \text{null}(\mathcal{H}^2) = \text{null}(\mathcal{H}) \oplus \text{span}\left\{ \begin{bmatrix} \widehat{\Phi}_1 \\ \mathbf{0} \end{bmatrix}, \begin{bmatrix} \widehat{\Phi}_2 \\ \mathbf{0} \end{bmatrix} \right\}, \tag{2.24}$$

where $\widehat{\Phi}_j = \mathcal{H}_+^{-1}\Phi_j$, $j = 1, 2$ and

$$\text{null}(\mathcal{H}) = \text{span}\left\{ \begin{bmatrix} \mathbf{0} \\ \Phi_1 \end{bmatrix}, \begin{bmatrix} \mathbf{0} \\ \Phi_2 \end{bmatrix} \right\}.$$

The convergence of the non-zero eigenvalues depends heavily on the approximation accuracy of generalized nullspace that is associated with $\mathcal{H}$ [21]. Based on Theorem 2.5 and Remark 2.2, we obtain the generalized nullspace of $\mathcal{H}$, thus essentially improving the convergence and efficiency.

3. Numerical method

In this section, we will propose an efficient and spectral accurate numerical method to solve the BdG equations (2.14). Due to the presence of external trapping potential $V(\boldsymbol{x})$, the ground states $\Phi_g(\boldsymbol{x})$ and the eigenfunctions $(\boldsymbol{u}, \boldsymbol{v})/(\boldsymbol{f}, \boldsymbol{g})$ are all smooth and fast decaying. Therefore, it is reasonable to truncate the whole space $\mathbb{R}^d$ into a bounded domain $\Omega \subset \mathbb{R}^d$ that is large enough such that truncation error is negligible. Since all related functions are smooth, the Fourier pseudospectral (FS) discretization stands out as the optimal candidate for spatial discretization [5, 6, 33], due to its simplicity, spectral accuracy, and great efficiency that is guaranteed by discrete Fast Fourier transform (FFT). The computation domain is usually chosen as a rectangle, denoted as $\mathcal{D}_L := [-L, L]^d$. Spatial discretization details will be presented in the next subsection.

3.1. Spatial discretization by Fourier spectral method

Provided that the stationary states Φ_g and all chemical potentials are precomputed with a very fine mesh by the gradient flow with Lagrange multiplier (GFLM) method [22], such that the numerical accuracy approaches machine precision. For simplicity, we choose to illustrate the spatial discretization for the 1D case and extensions to higher dimensions are omitted here. We choose the computational domain $\mathcal{D}_L := [-L, L]$ and discretize it uniformly with mesh size $h_x = \frac{2L}{N}$ where N is a positive even integer. Define the grid point set as $\mathcal{T}_x = \{(-N/2, \cdots, N/2)h_x\}$ and introduce the plane wave basis and discrete space as

$$W_k(x) = e^{i\mu_k(x+L)} \quad (-N/2 \leq k \leq N/2 - 1), \text{ and } X_N = \text{span}\{W_k(x)\}_{k=-N/2}^{N/2-1},$$

with $\mu_k = \pi k / L$. Define $F(x_n)$ $(F = \phi_j^g, u_j, v_j, V$ etc.) as function value at grid point $x_n = -L + nh_x \in \mathcal{T}_x$ and $\mathbf{F} = (F(x_1), F(x_2), \cdots, F(x_N))$ as the corresponding discrete vector. The Fourier pseudo-spectral approximations of F, denoted by F_N, and its Laplacian $\nabla^2 F$ read as follows

$$F(x) \approx (\mathcal{I}_N F)(x) := \sum_{k=-N/2}^{N/2-1} \widetilde{F}_k \, W_k(x), \quad (\nabla^2 F)(x) \approx (\nabla^2 (\mathcal{I}_N F))(x) = \sum_{k=-N/2}^{N/2-1} -\mu_k^2 \, \widetilde{F}_k \, W_k(x),$$

where $\mathcal{I}_N$ denotes a mapping from $C(\Omega)$ to X_N, and $\widetilde{F}_k$, the discrete Fourier transform of vector $\mathbf{F}$, is computed as

$$\widetilde{F}_k = \frac{1}{N} \sum_{n=0}^{N-1} F(x_n) \overline{W}_k(x_n) = \frac{1}{N} \sum_{n=0}^{N-1} F(x_n) \, e^{\frac{-i2\pi nk}{N}}, \qquad -N/2 \leq k \leq N/2 - 1, \qquad (3.1)$$

and is accelerated by discrete Fast Fourier transform (FFT) within $O(N \ln(N))$ float operations. The numerical approximation of Laplacian operator ∇^2, denoted as $[\![\nabla^2]\!]$, corresponds to a dense matrix [28, 33, 38]. We map the function's pointwise multiplication $F_n G_n$ as a matrix-vector product $[\![F]\!]\mathbf{G}$, that is,

$$([\![F]\!]\mathbf{G})_n := F_n G_n \quad \Longrightarrow \quad [\![F]\!] = \text{diag}(\mathbf{F}). \qquad (3.2)$$

Therefore, operators $\mathcal{A}$ and $\mathcal{B}$ are mapped into matrices $\mathbf{A}$ and $\mathbf{B}$ in the following way

$$\mathbf{A} := [\![L\mathbf{I}_3 - \Lambda]\!] + \beta_n\left([\![\rho\mathbf{I}_3]\!] + [\![\Phi_g \Phi_g^\top]\!]\right) + \beta_s\left([\![\mathbf{S} \cdot \mathbf{s}(\Phi_g)]\!] + \sum_{j=x,y,z} [\![\mathbf{S}_j \Phi_g \Phi_g^\top \mathbf{S}_j]\!]\right), \quad (3.3)$$

$$\mathbf{B} := \beta_n [\![\Phi_g \Phi_g^\top]\!] + \beta_s \sum_{j=x,y,z} [\![\mathbf{S}_j \Phi_g \Phi_g^\top \mathbf{S}_j^\top]\!]. \qquad (3.4)$$

Thanks to the Fourier spectral discretization, both matrices $\mathbf{A}$ and $\mathbf{B}$ are symmetric, thus keeping their continuous operators' Hermitian property. Setting $\boldsymbol{u}_N = (\boldsymbol{u}_{1,N}; \boldsymbol{u}_{0,N}; \boldsymbol{u}_{-1,N})$ and $\boldsymbol{v}_N = (\boldsymbol{v}_{1,N}; \boldsymbol{v}_{0,N}; \boldsymbol{v}_{-1,N})$, the BdG equations (2.12) are then discretized into a linear eigenvalue problem

$$\begin{bmatrix} \mathbf{A} & \mathbf{B} \\ -\mathbf{B} & -\mathbf{A} \end{bmatrix} \begin{bmatrix} \boldsymbol{u}_N \\ \boldsymbol{v}_N \end{bmatrix} = \omega_N \begin{bmatrix} \boldsymbol{u}_N \\ \boldsymbol{v}_N \end{bmatrix}. \qquad (3.5)$$

With a similar change of variables, i.e.,

$$\boldsymbol{f}_N = \frac{1}{2}(\boldsymbol{u}_N + \boldsymbol{v}_N), \; \boldsymbol{g}_N = \frac{1}{2}(\boldsymbol{u}_N - \boldsymbol{v}_N), \qquad (3.6)$$

the above equation is rewritten into a linear response eigenvalue problem

$$\begin{bmatrix} \mathbf{O} & \mathbf{H}_- \\ \mathbf{H}_+ & \mathbf{O} \end{bmatrix} \begin{bmatrix} \boldsymbol{f}_N \\ \boldsymbol{g}_N \end{bmatrix} = \omega_N \begin{bmatrix} \boldsymbol{f}_N \\ \boldsymbol{g}_N \end{bmatrix}, \tag{3.7}$$

where $\mathbf{H}_- = \mathbf{A} - \mathbf{B}$ and $\mathbf{H}_+ = \mathbf{A} + \mathbf{B}$.

The above discrete dense eigensystem (3.7) is solved using the recently developed BiOrthogonal Structure Preserving algorithm (BOSP for short) [21], and details are illustrated in the coming subsection.

Remark 3.1 (Matching eigenfunction constrain (2.15)). *In practice, we do not need to bother about the constrain (2.15) when solving the eigenvalue problem (3.7). Actually, once the eigenvectors are computed, the constrain (2.15) will be satisfied easily with a scalar scaling of $\boldsymbol{f}_N$ and $\boldsymbol{g}_N$.*

3.2. Bi-orthogonal structure-preserving Fourier spectral eigensolver

The ARPACK package has been successfully adapted to BdG equations of dipolar BEC [34, 33]. However, a similar adaptation attempt is not as effective, and sometimes it does not even converge within a reasonable time, because the generalized nullspace is much larger and more complicated, not to even mention the large-scale dense eigensystem for three-dimensional problems. The eigenspaces associated with eigenvalues of different magnitudes are biorthogonal, and such biorthogonality property shall be taken into account in the eigensolver design [2, 3, 21]. The structure of generalized nullspace and biorthogonality, well described in Section 2 on the continuous level, are assessed numerically by the linear algebra package (LAPACK) and a modified Gram-Schmidt biorthogonal algorithm. Based on the recently developed linear response eigensolver BOSP [21], by combing the Fourier spectral method for spatial approximation and making use of the specific generalized nullspace structure (Section 2.3), we propose an efficient iterative subspace eigensolver and provide a friendly interface for matrix-vector product evaluation. Since there is no explicit matrix storage and the matrix-vector product is implemented via FFT within almost optimal $O(\texttt{DOF}\log(\texttt{DOF}))$ operations ($\texttt{DOF}$ is the degree of freedom/total number of grid points, i.e., $\texttt{DOF} = N^d$), the heavy memory burden is much more alleviated and the computational efficiency is guaranteed to a large extent. Therefore, it provides a feasible solution to large-scale problems, especially in such a densely populated system in our case. Thanks to the Fourier spectral method, our solver can achieve spectral accuracy for both eigenvalue and eigenvectors as long as the BOSP's accuracy tolerance is chosen sufficiently small.

As is known, the matrix-vector product evaluation is the most time-consuming part. While, in this article, the matrix-vector product

$$\mathbf{H}_+ \boldsymbol{f}_N, \quad \mathbf{H}_- \boldsymbol{g}_N, \quad \text{for} \quad \boldsymbol{f}_N, \boldsymbol{g}_N \in \mathbb{R}^{3N},$$

can be realized by two pairs of FFT/iFFT plus some function multiplication in physical space. The overall computational costs to compute the first `nev` eigenpairs amounts to

$$\mathcal{O}(\texttt{nev}) \times \big(\mathcal{O}(\texttt{DOF}\log(\texttt{DOF})) + \mathcal{O}(\texttt{DOF})\big) + \mathcal{O}(\texttt{nev}^3) = \mathcal{O}(\texttt{nev}\, N \log(\texttt{DOF})) + \mathcal{O}(\texttt{nev}^3).$$

When the degree of freedom is much larger than the number of eigenvalues, i.e., $\texttt{DOF} \gg \texttt{nev}$, the computational costs are approximately $\mathcal{O}(\texttt{nev} \times \texttt{DOF}\log(\texttt{DOF}))$ and will be verified numerically in the next section.

13

3.3. Stability analysis

To demonstrate the practicality of our solver, we will present a rigorous stability analysis for the eigenfunctions in this subsection. Since the density and eigenfunction both decay fast enough in space, it is reasonable to assume that $\chi(\boldsymbol{x})$ $(\chi = \phi_j^g, u_j, v_j,$ etc.) is numerically compactly supported in a bounded domain $\Omega \subsetneq \mathbb{R}^d$, that is, $\mathrm{supp}\{\chi\} \subsetneq \Omega$. We introduce $2L$-periodic Sobolev space $H_p^m(\Omega) \subset H^m(\Omega)$ $(m \geq 1)$ with $\Omega = \mathcal{D}_L$, and the semi-norm, norm and ∞-norm as follows, respectively,

$$|\chi|_m := \left(\sum\nolimits_{|\boldsymbol{\alpha}|=m} \|\partial^{\boldsymbol{\alpha}}\chi\|^2\right)^{1/2}, \quad \|\chi\|_m := \left(\sum\nolimits_{|\boldsymbol{\alpha}|\leq m} \|\partial^{\boldsymbol{\alpha}}\chi\|^2\right)^{1/2}, \quad \|\chi\|_\infty = \sup_{\boldsymbol{x}\in\Omega} |\chi(\boldsymbol{x})|,$$

with index $\boldsymbol{\alpha} = (\alpha_1,\ldots,\alpha_d) \in \mathbb{Z}^d$, $|\boldsymbol{\alpha}| = \sum_{j=1}^d \alpha_j$, $\partial^{\boldsymbol{\alpha}} = \partial_{x_1}^{\alpha_1}\cdots\partial_{x_d}^{\alpha_d}$ and $\|\cdot\|$ being the L^2 norm. For vector-valued function $\boldsymbol{\chi} = (\chi_1, \chi_0, \chi_{-1})^\top$, we define $|\boldsymbol{\chi}|_m := \sqrt{\sum_{j=-1}^1 |\chi_j|_m^2}$, $\|\boldsymbol{\chi}\|_m := \sqrt{\sum_{j=-1}^1 \|\chi_j\|_m^2}$, $\|\boldsymbol{\chi}\| := \sqrt{\sum_{j=-1}^1 \|\chi_j\|^2}$, and $\|\boldsymbol{\chi}\|_\infty := \max\{\|\chi_j\|_\infty\}$. We use $A \lesssim B$ to denote $A \leq cB$ where the constant $c > 0$ is independent of the grid number N. Then we introduce the stability analysis as follows:

Theorem 3.1 (Stability Analysis). *For any $\boldsymbol{\chi}(\boldsymbol{x}) = (\chi_1(\boldsymbol{x}), \chi_0(\boldsymbol{x}), \chi_{-1}(\boldsymbol{x}))^\top \in (H_p^m(\Omega))^3$ with $m > d/2 + 2$, and its Fourier pseudo-spectral approximations*

$$(\mathcal{I}_N\boldsymbol{\chi})(\boldsymbol{x}) = \left((\mathcal{I}_N\chi_1)(\boldsymbol{x}), (\mathcal{I}_N\chi_0)(\boldsymbol{x}), (\mathcal{I}_N\chi_{-1})(\boldsymbol{x})\right)^\top,$$

we have the following error estimate

$$\|\mathcal{Q}\boldsymbol{\chi} - \mathcal{Q}(\mathcal{I}_N\boldsymbol{\chi})\|_\infty \;\lesssim\; N^{-(m-\frac{d}{2}-2)}, \tag{3.8}$$

where $\mathcal{Q} = \mathcal{A}, \mathcal{B}$, and $\boldsymbol{\chi} = \boldsymbol{u}, \boldsymbol{v}$.

To prove the above theorem, the following preparations are required.

Lemma 3.1 (Fourier spectral approximation [23, 28]). *For $\chi(\boldsymbol{x}) \in H_p^m(\Omega)$ with $m > d/2$, and its Fourier pseudo-spectral approximation $\mathcal{I}_N\chi$, we have the following error estimates*

$$\|\partial^{\boldsymbol{\alpha}}(\chi - \mathcal{I}_N\chi)\|_\infty \;\lesssim\; N^{-(m-\frac{d}{2}-|\boldsymbol{\alpha}|)}|\chi|_m, \qquad 0 \leq |\boldsymbol{\alpha}| \leq m, \tag{3.9}$$

$$\|\partial^{\boldsymbol{\alpha}}(\chi - \mathcal{I}_N\chi)\| \;\lesssim\; N^{-(m-|\boldsymbol{\alpha}|)}|\chi|_m, \qquad 0 \leq |\boldsymbol{\alpha}| \leq m. \tag{3.10}$$

Since operators $\mathcal{A}$ and $\mathcal{B}$ contain only two types of operators, namely, the Laplacian operator ∇^2 and function multiplication operation that involves $V(\boldsymbol{x})$ & $\phi_i^g\phi_j^g$, the following corollary is a prerequisite for proving Theorem 3.1.

Corollary 3.1. *For $\chi(\boldsymbol{x}) \in H_p^m(\Omega)$ with $m > d/2$, and its Fourier pseudo-spectral approximation $\mathcal{I}_N\chi$, we have*

$$\|\nabla^2\chi - \nabla^2(\mathcal{I}_N\chi)\|_\infty \;\lesssim\; N^{-(m-\frac{d}{2}-2)}|\chi|_m, \tag{3.11}$$

$$\|V\chi - V(\mathcal{I}_N\chi)\|_\infty \;\lesssim\; N^{-(m-\frac{d}{2})}|\chi|_m, \tag{3.12}$$

$$\|\phi_i^g\phi_j^g\chi - \phi_i^g\phi_j^g(\mathcal{I}_N\chi)\|_\infty \;\lesssim\; N^{-(m-\frac{d}{2})}|\chi|_m \quad (i,j=1,0,-1). \tag{3.13}$$

14

Since it is easy to prove the above corollary using Lemma 3.1 and we shall omit details for brevity.

The proof of Theorem 3.1:

Proof. For simplicity, we only prove the $\mathcal{Q} = \mathcal{A}$ case and extensions to other operators are similar. From (3.9)-(3.13), we obtain

$$\|(L\mathbf{I}_3 - \Lambda)\boldsymbol{\chi} - (L\mathbf{I}_3 - \Lambda)(\mathcal{I}_N\boldsymbol{\chi})\|_\infty \lesssim N^{-(m-\frac{d}{2}-2)}|\boldsymbol{\chi}|_m.$$

For the second and third terms of $\mathcal{A}$ as shown in Eqn. (2.5) (the same as $\mathbf{A}$ in (3.3)), using (3.9), (3.13) and triangle inequality, the following error estimate holds:

$$\left\|\left(\mathcal{A} - (L\mathbf{I}_3 - \Lambda)\right)\boldsymbol{\chi} - \left(\mathcal{A} - (L\mathbf{I}_3 - \Lambda)\right)(\mathcal{I}_N\boldsymbol{\chi})\right\|_\infty \lesssim N^{-(m-\frac{d}{2})}|\boldsymbol{\chi}|_m.$$

Therefore, we finish the proof of Theorem 3.1. □

3.4. Convergence analysis

In this subsection, we will propose the convergence analysis of Fourier pseudo-spectral approximations. To begin with, and adopt the Sobolev space $\mathbb{V} = (H_p^1(\Omega))^3 \times (H_p^1(\Omega))^3$ with the following norm

$$\|\boldsymbol{\Phi}\|_1 = \sqrt{\|\boldsymbol{f}\|_1^2 + \|\boldsymbol{g}\|_1^2} \quad \text{and} \quad \|\boldsymbol{\Phi}\| = \sqrt{\|\boldsymbol{f}\|^2 + \|\boldsymbol{g}\|^2}, \quad \forall\, \boldsymbol{\Phi} := (\boldsymbol{f}; \boldsymbol{g}) \in \mathbb{V}.$$

The BdG equation (2.14) is equivalent to the following eigenvalue problem:

$$\widetilde{\mathcal{H}} \begin{bmatrix} \boldsymbol{f} \\ \boldsymbol{g} \end{bmatrix} := \begin{bmatrix} \mathcal{H}_+ & \mathcal{O} \\ \mathcal{O} & \mathcal{H}_- \end{bmatrix} \begin{bmatrix} \boldsymbol{f} \\ \boldsymbol{g} \end{bmatrix} = \omega \begin{bmatrix} 0 & 1 \\ 1 & 0 \end{bmatrix} \begin{bmatrix} \boldsymbol{f} \\ \boldsymbol{g} \end{bmatrix} \tag{3.14}$$

The Galerkin weak form of Eqn. (3.14) reads as: to find $0 \neq \omega \in \mathbb{R}$ and $\boldsymbol{\Phi} = (\boldsymbol{f}; \boldsymbol{g}) \in \mathbb{V}$ such that

$$a(\boldsymbol{\Phi}, \boldsymbol{\Psi}) = \omega\, b(\boldsymbol{\Phi}, \boldsymbol{\Psi}), \quad \forall\, \boldsymbol{\Psi} = (\boldsymbol{\xi}; \boldsymbol{\eta}) \in \mathbb{V}, \tag{3.15}$$

subject to constraint $b(\boldsymbol{\Phi}, \boldsymbol{\Phi}) = 1/2$ with

$$a(\boldsymbol{\Phi}, \boldsymbol{\Psi}) := \langle \mathcal{H}_+ \boldsymbol{f}, \boldsymbol{\xi} \rangle + \langle \mathcal{H}_- \boldsymbol{g}, \boldsymbol{\eta} \rangle, \quad b(\boldsymbol{\Phi}, \boldsymbol{\Psi}) := \langle \boldsymbol{g}, \boldsymbol{\xi} \rangle + \langle \boldsymbol{f}, \boldsymbol{\eta} \rangle,$$

where $\langle \boldsymbol{f}, \boldsymbol{g} \rangle := \sum_{j=-1}^1 \int_{\mathbb{R}^d} f_j(\boldsymbol{x})\overline{g_j(\boldsymbol{x})}\, \mathrm{d}\boldsymbol{x}, \; \forall\, \boldsymbol{f}, \boldsymbol{g} \in (L^2(\Omega))^3$.

Remark 3.2. *From Theorem 2.5 or Remark 2.2, we can prove that there exists $c_0 > 0$ such that*

$$a(\boldsymbol{\Phi}, \boldsymbol{\Phi}) \geq c_0\|\boldsymbol{\Phi}\|_1, \quad \forall\, \boldsymbol{\Phi} \in \mathbb{U}, \tag{3.16}$$

where the subspace $\mathbb{U}$ is defined as

$$\mathbb{U} = \mathrm{null}(\mathcal{H}_+)^\perp \times \mathrm{null}(\mathcal{H}_-)^\perp \subset \mathbb{V},$$

with $\mathrm{null}(\mathcal{H}_\pm)^\perp := \{\boldsymbol{f} \in (H_p^1(\Omega))^3 \,|\, \langle \boldsymbol{f}, \boldsymbol{\xi} \rangle = 0, \; \forall\, \boldsymbol{\xi} \in \mathrm{null}(\mathcal{H}_\pm)\}$. It is important to point out that solving the BdG equation (3.15) in $\mathbb{U}$ is equivalent to solving non-zero ω and its associated eigenfunction $\boldsymbol{\Phi}$ in $\mathbb{V}$.

Define the approximation finite dimensional spaces X_N of $H_p^1(\Omega)$ and $\mathbb{V}_N$ of $\mathbb{V}$ as follows:

$$X_N := \operatorname{span}\left\{W_k(\boldsymbol{x}), k = -N/2, \ldots, N/2 - 1\right\}, \quad \mathbb{V}_N := (X_N)^3 \times (X_N)^3,$$

and consider its approximation problem: to find $0 \neq \omega_N \in \mathbb{R}$ and $\boldsymbol{\Phi}_N = (\boldsymbol{f}_N; \boldsymbol{g}_N) \in \mathbb{V}_N$ such that

$$a_N(\boldsymbol{\Phi}_N, \boldsymbol{\Psi}_N) = \omega_N \, b_N(\boldsymbol{\Phi}_N, \boldsymbol{\Psi}_N), \quad \forall \boldsymbol{\Psi}_N = (\boldsymbol{\xi}_N; \boldsymbol{\eta}_N) \in \mathbb{V}_N, \tag{3.17}$$

subject to normalization constraint $b_N(\boldsymbol{\Phi}_N, \boldsymbol{\Phi}_N) = 1/2$ with

$$a_N(\boldsymbol{\Phi}_N, \boldsymbol{\Psi}_N) = \langle \mathcal{H}_+ \boldsymbol{f}_N, \boldsymbol{\xi}_N \rangle_N + \langle \mathcal{H}_- \boldsymbol{g}_N, \boldsymbol{\eta}_N \rangle_N, \quad b_N(\boldsymbol{\Phi}_N, \boldsymbol{\Psi}_N) = \langle \boldsymbol{g}_N, \boldsymbol{\xi}_N \rangle_N + \langle \boldsymbol{f}_N, \boldsymbol{\eta}_N \rangle_N,$$

and $\langle \boldsymbol{f}, \boldsymbol{\xi} \rangle_N := \sum_{j=-1}^{1} \left\langle f_j^N, \xi_j^N \right\rangle_N := \sum_{j=-1}^{1} \left(\frac{2L}{N} \sum_{n=0}^{N} f_j^N(\boldsymbol{x}_n) \overline{g_j^N(\boldsymbol{x}_n)} \right)$.

Similar as Lemma A.1, we have the following equivalence result and choose to omit proofs for brevity.

Lemma 3.2. *The discrete problem* (3.7) *and discrete variational problem* (3.17) *are equivalent.*

To illustrate the convergence behavior, we introduce the following notation

$$\delta_N(\boldsymbol{\Phi}) = \inf_{\boldsymbol{\Psi} \in \mathbb{V}_N} \left\{ \|\boldsymbol{\Phi} - \boldsymbol{\Psi}\|_1 + \sup_{\boldsymbol{\Theta} \in \mathbb{V}_N} \frac{|a(\boldsymbol{\Psi}, \boldsymbol{\Theta}) - a_N(\boldsymbol{\Psi}, \boldsymbol{\Theta})|}{\|\boldsymbol{\Theta}\|_1} \right\}. \tag{3.18}$$

Similar as Lemma A.2 for scalar function, by the coerciveness of bilinear operator $a(\cdot, \cdot)$ (Eqn. (3.16)) and the conformal subspace approximation, we obtain

$$\delta_N(\boldsymbol{\Phi}) \lesssim N^{-(m-\sigma)}, \quad \text{with} \quad \sigma = \max\{1, d/2\}. \tag{3.19}$$

According to the general theory given by Lemma A.3, we derive the following error estimates.

Lemma 3.3. *For any eigenpair approximation* $\{\omega_N; \boldsymbol{\Phi}_N\}$ *of Eqn.* (3.17), *there is an eigenpair* $\{\omega; \boldsymbol{\Phi}\}$ *of Eqn.* (3.15) *corresponding to* ω *such that*

$$\|\boldsymbol{\Phi} - \boldsymbol{\Phi}_N\|_1 \lesssim \delta_N(\boldsymbol{\Phi}), \quad \|\boldsymbol{\Phi} - \boldsymbol{\Phi}_N\| \lesssim \zeta_N \|\boldsymbol{\Phi} - \boldsymbol{\Phi}_N\|_1, \quad |\omega - \omega_N| \lesssim \|\boldsymbol{\Phi} - \boldsymbol{\Phi}_N\|_1^2,$$

where the constant ζ_N *approaches* 0 *as* $N \to \infty$.

Finally, via a change of variables, i.e., Eqn (2.13) and (3.6), we obtain error estimates for $(\boldsymbol{u}, \boldsymbol{v})$.

Theorem 3.2 (**Error Estimates**). *If* $\boldsymbol{u}, \boldsymbol{v} \in (H_p^m(\Omega))^3$ *with* $m \geq 1$ *and* $\operatorname{supp}\{\boldsymbol{u}\}, \operatorname{supp}\{\boldsymbol{v}\} \subsetneq \Omega$, *then for any eigenpair approximation* $\{\omega_N; \boldsymbol{u}_N, \boldsymbol{v}_N\}$ *of* (3.5), *there is an eigenpair* $\{\omega; \boldsymbol{u}, \boldsymbol{v}\}$ *of Eqn.* (2.12) *satisfying the following error estimates*

$$\begin{aligned} \|\boldsymbol{u} - \boldsymbol{u}_N\| + \|\boldsymbol{v} - \boldsymbol{v}_N\| &\lesssim N^{-(m-\sigma)}, \\ |\omega - \omega_N| &\lesssim N^{-2(m-\sigma)}, \end{aligned}$$

where $\sigma = \max\{1, d/2\}$.

4. Numerical results

In this section, we first carry out comprehensive numerical studies to illustrate the accuracy and efficiency of our solver. Then we apply it to investigate the Bogoliubov excitations around the ground states of spin-1 BEC. The ground states Φ_g and the chemical potentials are precomputed with accuracy close to machine precision via GFLM method [22] in a large enough domain with a small enough mesh size. Unless stated otherwise, we choose the potential $V(\boldsymbol{x})$ as the harmonic trapping potential (1.2) and set the computational domain as squares and $L = 16$ for 1D & 2D and $L = 8$ for 3D respectively, i.e., $\mathcal{D} = [-16, 16]$ in 1D, $\mathcal{D} = [-16, 16]^2$ in 2D and $\mathcal{D} = [-8, 8]^3$ in 3D respectively. The domain is discretized uniformly in each spatial direction with the same mesh size $h = 2L/N$ for simplicity. We choose to study the ferromagnetic (**FM** for short) case with $\beta_n = 885.4$, $\beta_s = -4.1$ and antiferromagnetic (**Anti-FM** for short) case with $\beta_n = 240.8$, $\beta_s = 7.5$ throughout the whole section.

4.1. Performance investigation

Firstly we verify the spectral accuracy for different space dimensions. Analytical eigenvalues and eigenvectors were given for harmonic trapping potential by equation (2.16) in Theorem 2.2. For an eigenvalue ω with multiplicity k, we denote its associated analytical eigenspaces as $\mathcal{M}_{\boldsymbol{u}} := \text{span}\{\boldsymbol{u}_1, \cdots, \boldsymbol{u}_k\}$, $\mathcal{M}_{\boldsymbol{v}} := \text{span}\{\boldsymbol{v}_1, \cdots, \boldsymbol{v}_k\}$, and denote $\{\omega_{\alpha,N}; \boldsymbol{u}_{\alpha,N}, \boldsymbol{v}_{\alpha,N}\}$ as the numerical approximations of eigenvalue ω_α and eigenfunctions $(\boldsymbol{u}_\alpha, \boldsymbol{v}_\alpha)$ obtained with mesh size $h = 2L/N$. To demonstrate the convergence, we adopt the following error functions

$$e^h_{\omega_\alpha} := \frac{|\omega_{\alpha,N} - \omega_\alpha|}{|\omega_\alpha|}, \qquad e^{h,\alpha}_{\boldsymbol{uv}} := \frac{\|\boldsymbol{u}_{\alpha,N} - \mathcal{P}_{\boldsymbol{u}}\boldsymbol{u}_{\alpha,N}\|_2}{\|\boldsymbol{u}_{\alpha,N}\|_2} + \frac{\|\boldsymbol{v}_{\alpha,N} - \mathcal{P}_{\boldsymbol{v}}\boldsymbol{v}_{\alpha,N}\|_2}{\|\boldsymbol{v}_{\alpha,N}\|_2},$$

where $\alpha = x$ in 1D, $\alpha = x, y$ in 2D and $\alpha = x, y, z$ in 3D, $\|\cdot\|_2$ is the discrete l^2 norm and $\mathcal{P}_\nu$ ($\nu = \boldsymbol{u}, \boldsymbol{v}$) is the l^2-orthogonal projection operator into space $\mathcal{M}_\nu$. In both examples, we compute the first 40 eigenvalues and their eigenfunctions.

Example 1 (**Accuracy**). *We study the accuracy convergence for both ferromagnetic and antiferromagnetic cases in 1D/2D/3D. To this end, we consider the following four cases*

   Case I. *1D case:* $\gamma_x = 1$.

   Case II. *Isotropic 2D case:* $\gamma_x = \gamma_y = 1$.

   Case III. *Anisotropic 2D case:* $\gamma_x = \gamma_y/2 = 1$.

   Case IV. *Isotropic 3D case:* $\gamma_x = \gamma_y = \gamma_z = 1$.

For **Case I**, there exists one analytical eigenvalue $\omega_x = 1$ with multiplicity $k = 1$. For **Case II**, there exist two analytical eigenvalues $\omega_x = \omega_y = 1$ with multiplicity $k = 2$. For **Case III**, $\omega_x = 1$ and $\omega_y = 2$ are eigenvalues with the same multiplicity $k = 1$. Similarly, for **Case IV**, there exist three analytical eigenvalues $\omega_x = \omega_y = \omega_z = 1$ with $k = 3$. Table 1-4 illustrate the numerical errors of eigenvalues and eigenvectors computed with different mesh sizes h in **Case I–IV**.

Table 1: Errors of the eigenvalue/eigenvector for **Case I** in **1D** for **FM** (upper) and **Anti-FM** cases (lower) in Example 1.

		$h_0 = 1$	$h_0/2$	$h_0/4$	$h_0/8$	$h_0/16$
FM	$e^h_{\omega_x}$	4.392E-03	9.570E-05	2.422E-08	1.383E-09	1.648E-12
	$e^{h,x}_{\boldsymbol{uv}}$	1.069E-01	1.234E-03	2.911E-06	4.481E-08	1.165E-12
Anti-FM	$e^h_{\omega_x}$	6.103E-02	1.831E-04	3.283E-10	6.677E-13	3.020E-14
	$e^{h,x}_{\boldsymbol{uv}}$	9.106E-01	1.156E-03	1.027E-06	1.609E-12	2.677E-12

Table 2: Errors of the eigenvalue/eigenvector for **Case II** in **2D** for **FM** (upper) and **Anti-FM** cases (lower) in Example 1.

		$h_0 = 1$	$h_0/2$	$h_0/4$	$h_0/8$	$h_0/16$
FM	$e^h_{\omega_x}$	6.022E-03	1.685E-05	7.811E-11	7.896E-13	5.014E-13
	$e^h_{\omega_y}$	6.022E-03	1.685E-05	7.812E-11	8.007E-13	4.925E-13
	$e^{h,x}_{\boldsymbol{uv}}$	3.503E-02	8.927E-04	4.250E-07	4.627E-08	2.751E-10
	$e^{h,y}_{\boldsymbol{uv}}$	3.506E-02	8.928E-04	4.250E-07	2.625E-08	2.751E-10
Anti-FM	$e^h_{\omega_x}$	6.825E-03	1.907E-05	4.664E-10	1.281E-12	4.241E-13
	$e^h_{\omega_y}$	6.825E-03	1.907E-05	2.822E-11	1.789E-11	4.607E-13
	$e^{h,x}_{\boldsymbol{uv}}$	5.013E-02	7.403E-04	1.558E-07	4.135E-10	1.147E-12
	$e^{h,y}_{\boldsymbol{uv}}$	5.006E-02	7.403E-04	1.555E-07	5.368E-10	1.416E-12

Table 3: Errors of the eigenvalue/eigenvector for **Case III** in **2D** for **FM** (upper) and **Anti-FM** cases (lower) in Example 1.

		$h_0 = 1$	$h_0/2$	$h_0/4$	$h_0/8$	$h_0/16$
FM	$e^h_{\omega_x}$	9.823E-03	1.153E-05	2.936E-11	2.138E-10	3.044E-12
	$e^h_{\omega_y}$	2.185E-02	1.514E-03	7.471E-08	6.092E-10	1.598E-12
	$e^{h,x}_{\boldsymbol{uv}}$	2.644E-02	8.649E-04	6.728E-07	1.398E-08	6.398E-09
	$e^{h,y}_{\boldsymbol{uv}}$	1.077	9.706E-03	3.186E-05	4.781E-08	3.306E-09
Anti-FM	$e^h_{\omega_x}$	7.222E-03	3.431E-05	1.844E-10	3.888E-13	8.724E-13
	$e^h_{\omega_y}$	4.328E-02	5.590E-04	4.039E-08	1.648E-13	4.867E-13
	$e^{h,x}_{\boldsymbol{uv}}$	3.484E-02	8.149E-04	2.777E-07	1.562E-12	7.409E-11
	$e^{h,y}_{\boldsymbol{uv}}$	1.738E-01	9.128E-03	1.706E-05	4.258E-11	7.208E-12

Table 4: Errors of the eigenvalue/eigenvector for **Case IV** in **3D** for **FM** (upper) and **Anti-FM** cases (lower) in Example 1.

		$h_0 = 1$	$h_0/2$	$h_0/4$	$h_0/8$
FM	$e^h_{\omega_x}$	3.526E-03	6.684E-06	6.108E-11	1.027E-11
	$e^h_{\omega_y}$	3.526E-03	6.684E-06	7.500E-12	1.028E-11
	$e^h_{\omega_z}$	3.526E-03	6.684E-06	4.598E-11	1.028E-11
	$e^{h,x}_{uv}$	4.434E-02	6.697E-04	1.116E-07	4.046E-09
	$e^{h,y}_{uv}$	4.433E-02	6.697E-04	1.116E-07	4.046E-09
	$e^{h,z}_{uv}$	4.443E-02	6.697E-04	1.116E-07	4.046E-09
Anti-FM	$e^h_{\omega_x}$	2.061E-03	3.620E-06	1.602E-11	8.528E-13
	$e^h_{\omega_y}$	2.061E-03	3.620E-06	1.213E-12	5.934E-13
	$e^h_{\omega_z}$	2.061E-03	3.620E-06	3.218E-11	5.874E-13
	$e^{h,x}_{uv}$	5.726E-02	5.812E-04	5.043E-08	5.873E-11
	$e^{h,y}_{uv}$	5.712E-02	5.812E-04	5.042E-08	5.873E-11
	$e^{h,z}_{uv}$	5.713E-02	5.812E-04	5.043E-08	5.873E-11

For the antiferromagnetic case in **Case I**, the convergence rates are compared between our proposed algorithm and LOBP4dCG [2, 3]. To address the positive semi-definiteness of the operator $\mathcal{H}_-$, a shift technique is employed for LOBP4dCG with a shift value of 10 so to achieve optimal convergence performance. Figure 4.1 shows the residual decay curves of the first six smallest eigenvalues $(\lambda_1, ..., \lambda_6)$ corresponding to the two algorithms. It can be seen that our algorithm converges faster than LOBP4dCG.
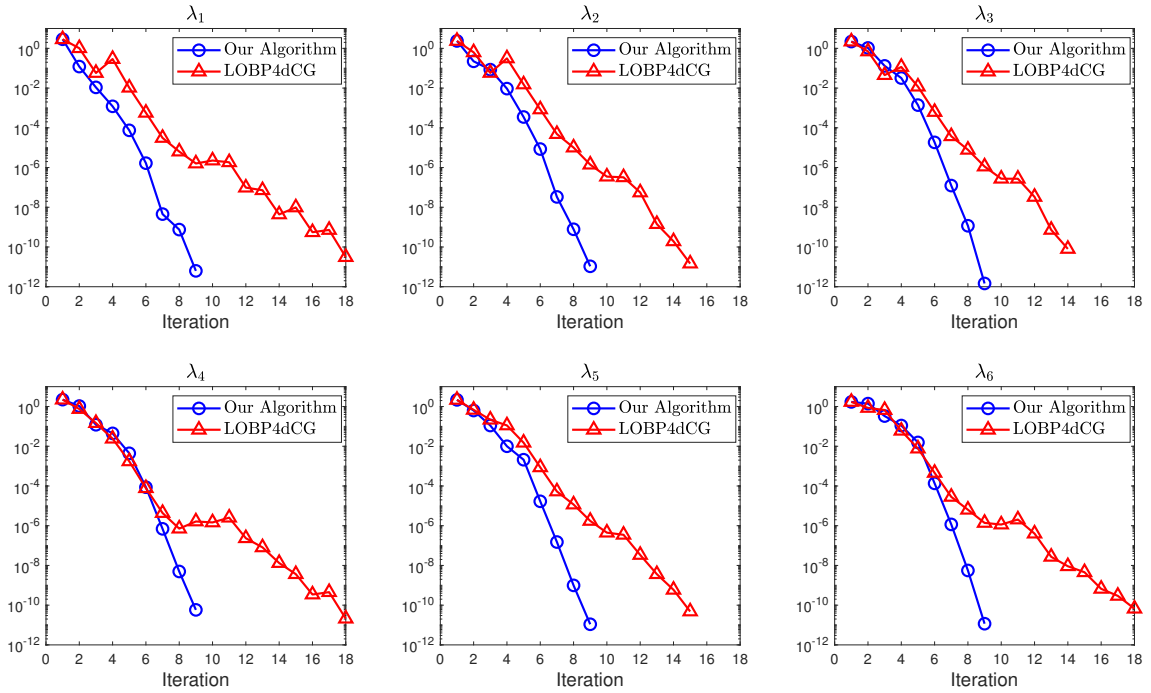
Figure 4.1: Descending trend of the normalized residuals in Example 1.
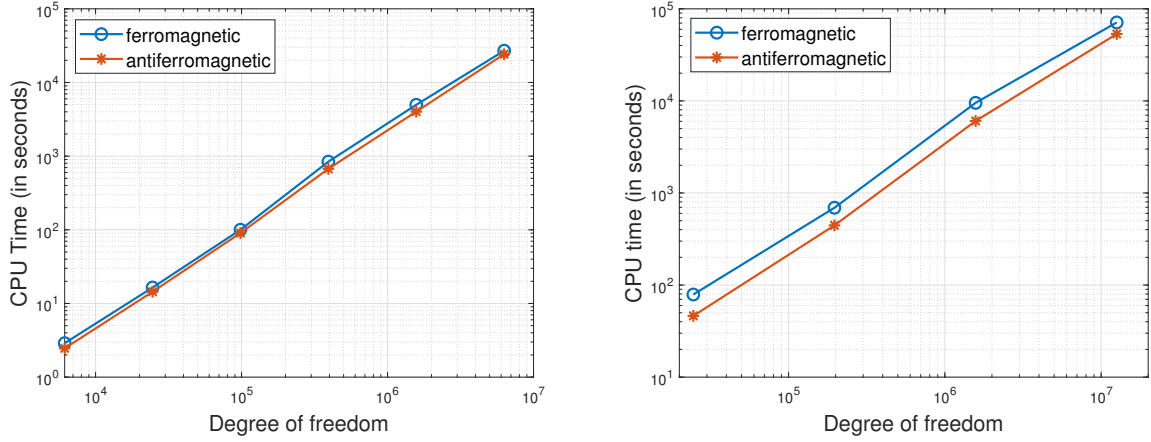
Figure 4.2: The computational times for **Case I** in **2D** (left) and **Case II** in **3D** (right) in Example 2.

Example 2 (**Efficiency**). *We investigate the efficiency performance using different mesh sizes for ferromagnetic and antiferromagnetic cases in 2D and 3D. To this end, we consider the following cases*

Case I. *Isotropic 2D case:* $\gamma_x = \gamma_y = 1$.

Case II. *Isotropic 3D case:* $\gamma_x = \gamma_y = \gamma_z = 1$.

Figure 4.2 presents the computation times (measured in seconds) versus the degree of freedom for 2D and 3D cases. The degree of freedom varies `DOF` = 6 144, 24 576, 98 304, 393 216, 1 572 864, 6 291 456 in 2D, and `DOF` = 24 576, 196 608, 1 572 864, 12 582 912 in 3D, while the number of eigenvalue is kept unchanged as `nev` = 40. It is obvious that the degree of freedom is much larger than the number of eigenvalues, i.e., `DOF` $\gg$ `nev`, therefore, the overall computational complexity is around $\mathcal{O}(\texttt{DOF}\log(\texttt{DOF}))$, which can be observed quite clear from Figure 4.2. Given the fact that the discrete BdG system is nonsymmetric and dense and the first `nev` = 40 eigenpairs of 3D problem can be computed with a **12 million** degree of freedom **within hours** using only solely sequentially one-CPU computing, it is reasonable to expect a promising future in physical applications.
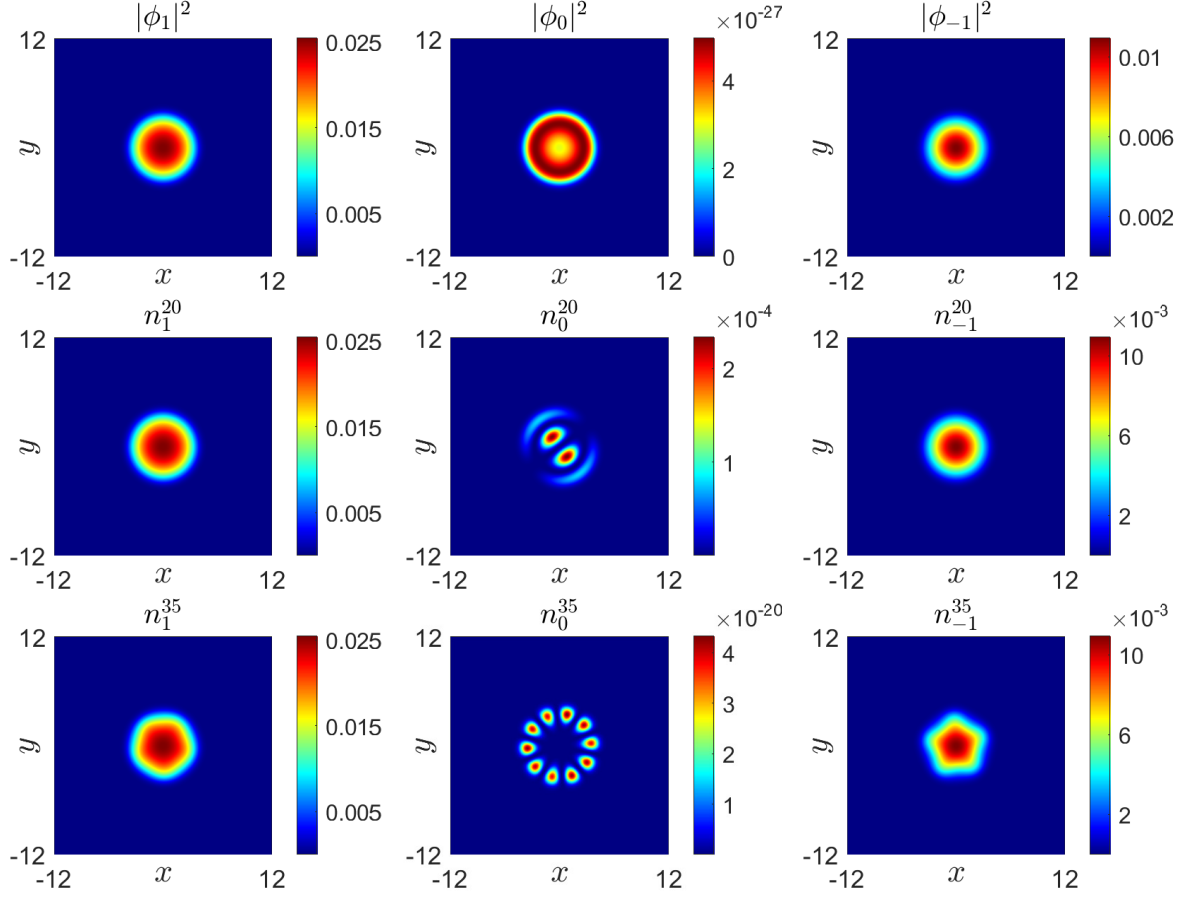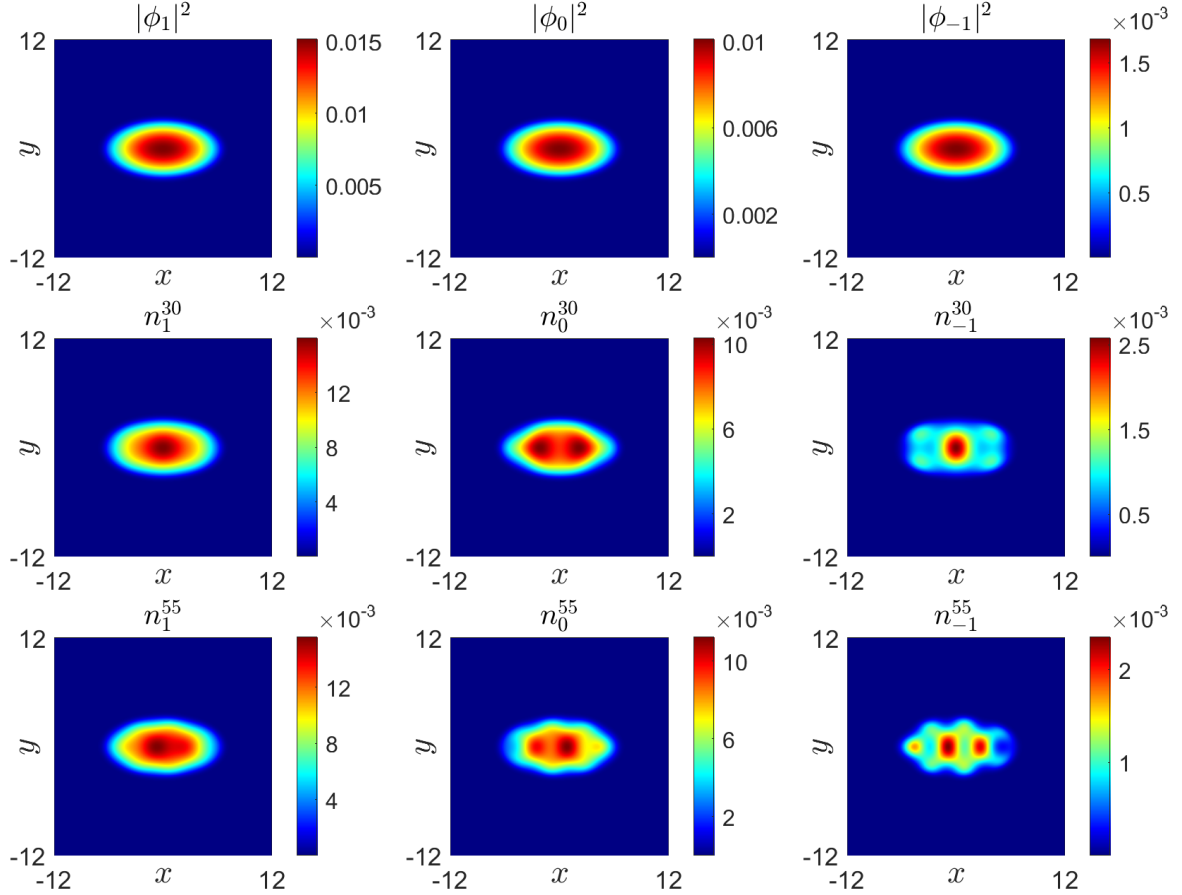
Figure 4.3: Snapshots of $|\phi_j(\boldsymbol{x})|^2$ (top row) and perturbed densities $n_j^\ell(\boldsymbol{x}, t = 10.6)$ by different excitation modes: $\ell = 20, 35$ (middle and bottom row) for **Case I** in Example 3 ($j = 1, 0, -1$ from left to right).

In this section, we apply our solver to investigate the excitation spectrum and Bogoliubov amplitudes of spin-1 BEC around the ground state. To visualize a normal mode, similar to (2.1), we analyze the evolution of the perturbed density profile [18]

$$n_j^\ell(\boldsymbol{x}, t) = \left|\left[\phi_j(\boldsymbol{x}) + \varepsilon\left(u_j^\ell(\boldsymbol{x})e^{-i\omega_\ell t} + \bar{v}_j^\ell(\boldsymbol{x})e^{i\omega_\ell t}\right)\right]\right|^2, \quad j = 0, \pm 1, \tag{4.1}$$

which reveals the nature of the excitations with ℓ being the eigenpair index. To this end, we choose a very fine mesh size $h = 1/8$ in both two and three spatial dimensions.

Example 3 (**2D Case**). *We investigate the perturbed density by different excitation modes in ferromagnetic and antiferromagnetic condensates in 2D. To this end, we choose $\varepsilon = 0.1$ and consider the following cases*

   Case I. *Isotropic antiferromagnetic condensates: $\gamma_x = \gamma_y = 1$, $\ell = 20, 35$.*

   Case II. *Anisotropic ferromagnetic condensates: $\gamma_x = \gamma_y/2 = 1$, $\ell = 30, 55$.*

Figure 4.3-4.4 displays the numerical excitations $n_j^\ell(\boldsymbol{x}, t)$ of the BdG equations (at $t = 10.6$) that are associated with the eigenvalues ω_ℓ for **Case I–II**. From these figures, we can see that both the spinor and external potential affect the shape of the excitations essentially and significantly. The eigenmodes $(\boldsymbol{u}^\ell, \boldsymbol{v}^\ell)$ are symmetric or antisymmetric in a symmetric or antisymmetric external potential, respectively. Meanwhile,

Figure 4.4: Snapshots of $|\phi_j(\boldsymbol{x})|^2$ (top row) and perturbed densities $n_j^\ell(\boldsymbol{x}, t = 10.6)$ by different excitation modes: $\ell = 30, 55$ (middle and bottom row) for **Case II** in Example 3 ($j = 1, 0, -1$ from left to right).

the eigenmodes will be compressed along the direction with a larger trapping frequency. Indeed, the presence of spinor and anisotropic external potential brings many more rich phase diagrams for eigenmodes of the BdG equations, which will be detailed in the future.

Example 4 (**3D Case**). *We study the Bogoliubov amplitudes of the BdG equations in ferromagnetic and antiferromagnetic condensates in 3D. To this end, we study the following four cases*

Case I. *Isotropic ferromagnetic condensates: $\gamma_x = \gamma_y = \gamma_z = 1$, $\ell = 25$.*

Case II. *Isotropic antiferromagnetic condensates: $\gamma_x = \gamma_y = \gamma_z = 1$, $\ell = 26$.*

Case III. *Anisotropic ferromagnetic condensates: $\gamma_x = \gamma_y = \gamma_z/2 = 1$, $\ell = 62$.*

Case IV. *Anisotropic antiferromagnetic condensates: $\gamma_x = \gamma_y = \gamma_z/2 = 1$, $\ell = 42$.*
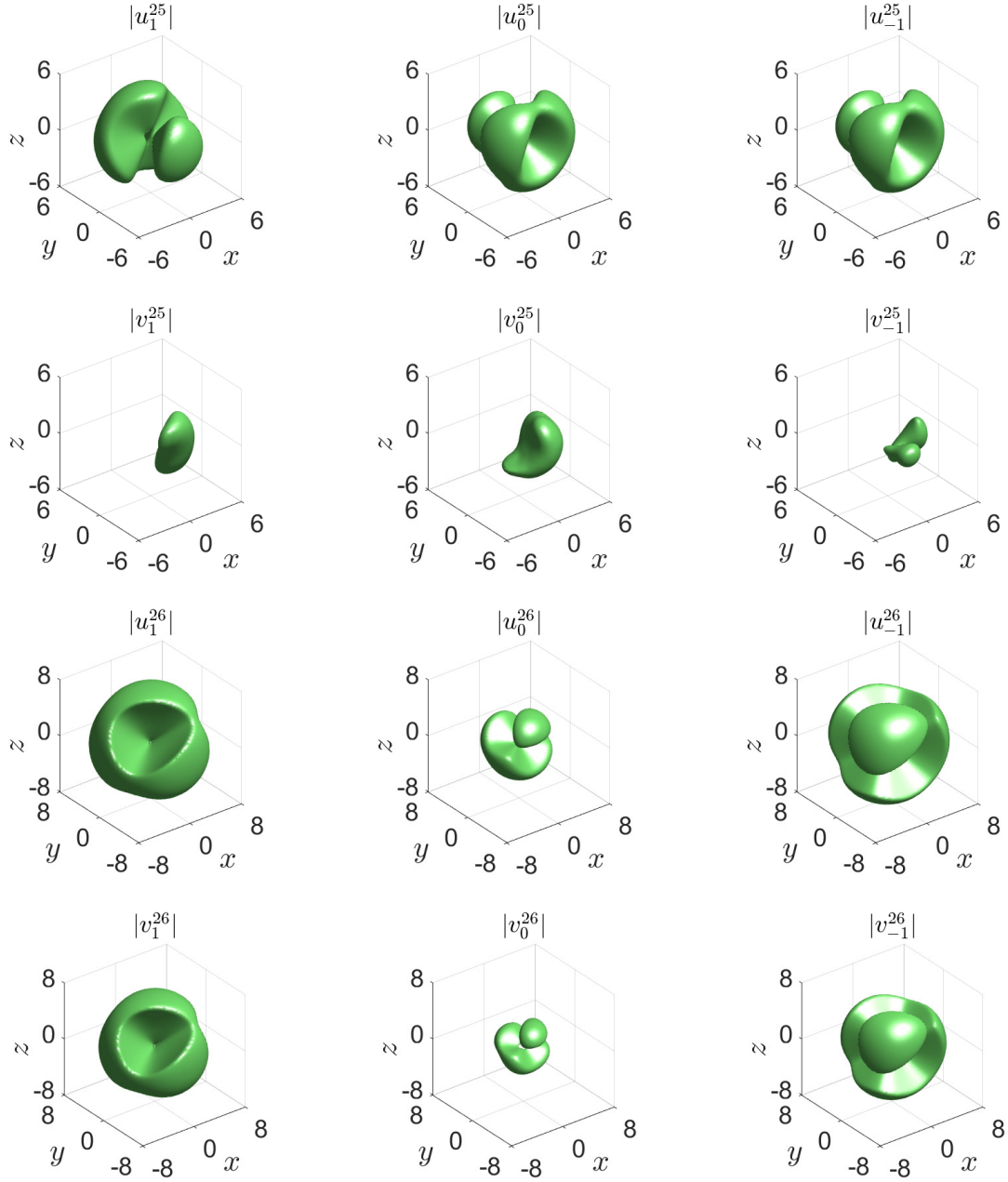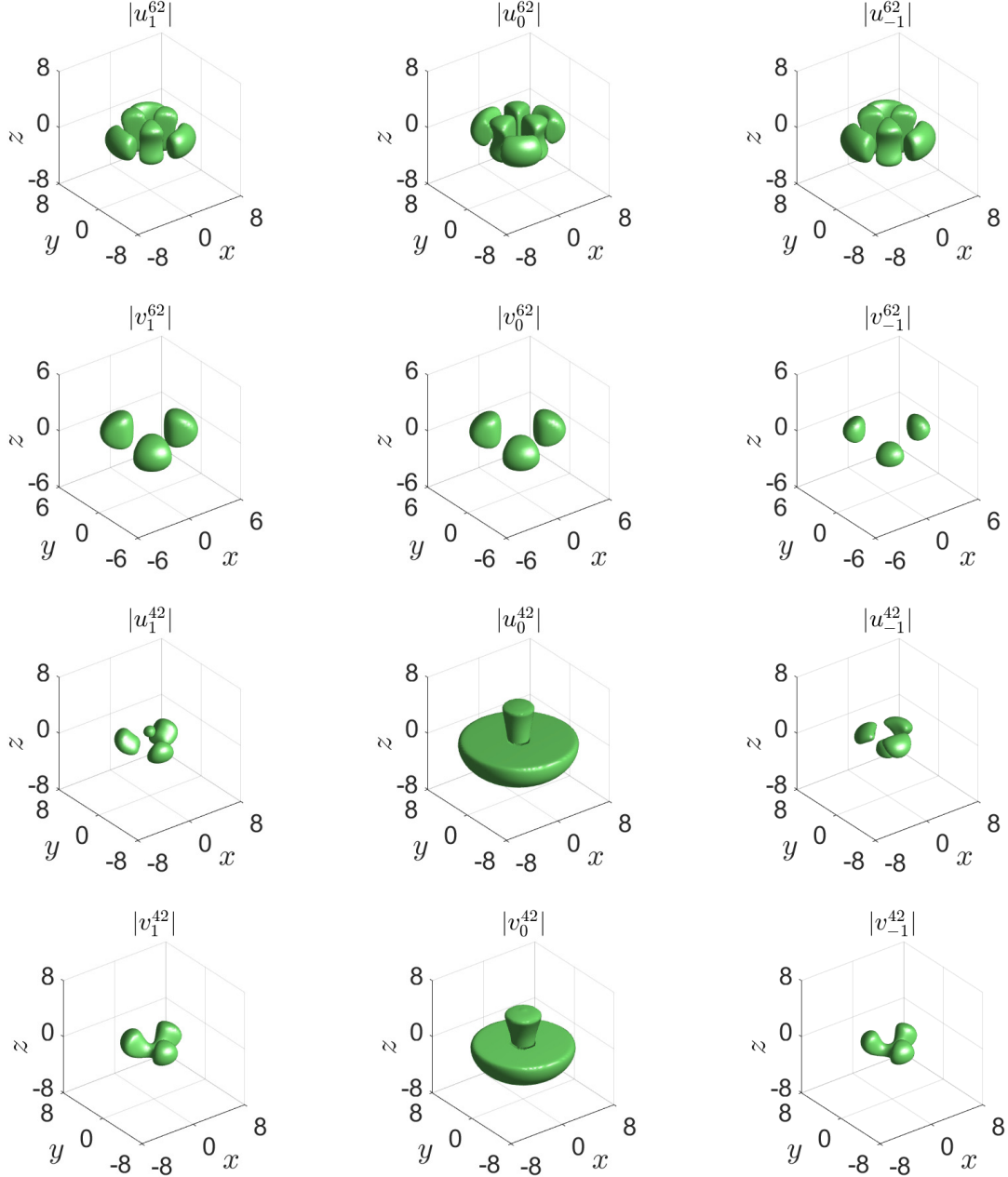
Figure 4.5: In Example 4, isosurface plots of the Bogoliubov amplitudes for **Case I**: $|u_j^{25}| = 10^{-3}$ (1st row), $|v_j^{25}| = 10^{-11}$ (2nd row), and **Case II**: $|u_j^{26}| = 10^{-10}$ (3rd row), $|v_j^{26}| = 10^{-11}$ (4th row) (from left to right: $j = 1, 0, -1$).

Figure 4.5–4.6 display isosurface plots of the eigenmodes $\boldsymbol{u}^\ell = (u_1^\ell, u_0^\ell, u_{-1}^\ell)^\top$ and $\boldsymbol{v}^\ell = (v_1^\ell, v_0^\ell, v_{-1}^\ell)^\top$ associated with the different ℓ for **Case I–IV**. From these figures, we can see that the external potential affects the shape of the eigenmodes $\boldsymbol{u}^\ell$ and $\boldsymbol{v}^\ell$ essentially and significantly. The eigenmodes can be symmetric or antisymmetric even in a symmetric trapping potential. Meanwhile, all eigenmodes will be compressed along the direction with a larger trapping frequency. For the 3D case, the presence of spinor and anisotropic external potential brings in many rich phase diagrams for eigenmodes, and we shall leave them as a future study.

Figure 4.6: In Example 4, isosurface of the Bogoliubov amplitudes for **Case III**: $|u_j^{62}| = 10^{-3}$ (1st row), $|v_j^{62}| = 10^{-12}$ (2nd row), and **Case IV**: $|u_j^{42}| = 10^{-9}$ (3rd row), $|v_j^{42}| = 10^{-10}$ (4th row) (from left to right: $j = 1, 0, -1$).

24

5. Conclusion

We proposed an efficient and spectrally accurate solver for computing the BdG equations of the spin-1 BECs. We first investigated its analytical eigenpairs, the structure of the generalized nullspace, and the bi-orthogonal property of eigenspaces on a continuous level. Then, based on a stable Gram-Schmidt bi-orthogonal algorithm, making use of the generalized nullspace and Fourier spectral method, we develop a stable, efficient, and accurate eigensolver. The solver is matrix-free and the most time-consuming matrix-vector product can be accelerated with FFT achieving almost optimal complexity ($O(\text{DOF}\log(\text{DOF}))$ operations). Furthermore, we rigorously proved its numerical stability and spectral convergence. Extensive numerical results confirm the spectral accuracy, efficiency in different dimensions, and we investigated the excitation spectrum (eigenvalues) and Bogoliubov amplitudes (eigenfunctions) around the ground state with different parameters. Extensions to BdG excitations of other BECs, such as multi-component BEC, spinor-dipolar BEC, etc, are feasible with minor adaptations on the specific matrix-vector product.

Appendix A. Supplement to the convergence analysis

The coerciveness and conformal finite-dimension subspace approximation of the original BdG problem (i.e., Eqn. (3.16) and (3.18)) are essential properties to establish error estimates, therefore, without loss of generality, we shall consider the following equivalent but much simpler eigenvalue problem: to find $(\lambda, u) \in \mathbb{R} \times H_p^m(\Omega)$ such that

$$\mathcal{L}u := -\Delta u + \gamma(\boldsymbol{x})u = \lambda\, u, \tag{A.1}$$

with constraint $\|u\| = 1$ in one dimension space. Furthermore, we assume the operator $\mathcal{L}$ is symmetric positive semi-definite and $\gamma(\boldsymbol{x})$ is a smooth function. Extensions to high-dimensional (2D/3D) cases are straightforward and we shall omit them for brevity.

Define the following inner products:

$$a(u,v) = \langle \nabla u, \nabla v \rangle + \langle \gamma u, v \rangle, \quad b(u,v) = \langle u, v \rangle, \quad \forall\, u, v \in H_p^m(\Omega)$$

$$\langle u, v \rangle = \int_\Omega u\bar{v}\mathrm{d}x \ \text{ and } \ \langle \nabla u, \nabla v \rangle = \int_\Omega \nabla u \cdot \overline{\nabla v}\mathrm{d}x.$$

It is easy to prove that $a(\cdot, \cdot)$ is an inner product and coercive in $H_p^m(\Omega)$, that is,

$$a(v,v) \le C_a \|v\|_1^2, \quad \forall\, v \in H_p^m(\Omega),$$

where C_a is a constant. In cases where $\text{null}(\mathcal{L})$ is non-empty, we define $V := \text{null}(\mathcal{L})^\perp = \{v \in H_p^m(\Omega) \mid \langle v, w \rangle = 0, \ w \in \text{null}(\mathcal{L})\}$ as the orthogonal complementary subspace, and the coerciveness (V-ellipticity) is satisfied as

$$C_a \|v\|_1^2 \leq a(v, v), \quad \forall\, v \in V. \tag{A.2}$$

In this appendix, we are concerned only with nonzero eigenvalues and their corresponding eigenfunctions, that is, solving the following weak form of Eqn. (A.1): to find $(\lambda, u) \in \mathbb{R} \times V$ such that

$$a(u, v) = \lambda\, b(u, v), \quad \forall\, v \in V, \tag{A.3}$$

subject to constraint $b(u, u) = 1$.

From Lemma 3.1, we could define the approximation finite dimensional spaces:

$$V_N := X_N \cap V \subset V.$$

The spectral-collocation method for (A.1) amounts to finding $(\lambda_N, u_N) \in \mathbb{R} \times V_N$ such that

$$-\Delta u_N(x_n) + \gamma(x_n)\, u_N(x_n) = \lambda_N\, u_N(x_n), \quad 0 \leq n \leq N - 1, \tag{A.4}$$

with constraint $b(u_N, u_N) = 1$ and $x_n = -L + nh_x \in \mathcal{T}_{\boldsymbol{x}}$. For convergence analysis, it is necessary to consider the following approximation problem: find $(\lambda_N, u_N) \in \mathbb{R} \times V_N$ such that

$$a_N(u_N, v_N) = \lambda_N\, b_N(u_N, v_N), \quad \forall\, v_N \in V_N, \tag{A.5}$$

subject to constraint $b_N(u_N, u_N) = 1$ with

$$a_N(u_N, v_N) := \langle \nabla u_N, \nabla v_N \rangle_N + \langle \gamma\, u_N, v_N \rangle_N, \quad b_N(u_N, v_N) := \langle u_N, v_N \rangle_N,$$

$$\langle u, v \rangle_N := \frac{2L}{N} \sum_{n=0}^{N-1} u_N(x_n)\overline{v_N}(x_n), \quad \text{and} \quad \langle \nabla u_N, \nabla v_N \rangle_N := \frac{2L}{N} \sum_{n=0}^{N-1} \nabla u_N(x_n) \cdot \overline{\nabla v_N}(x_n).$$

Lemma A. 1. *The discrete problem* (A.4) *and discrete variational problem* (A.5) *are equivalent.*

Proof. Multiplying both sides of (A.4) by $\overline{W_j}(x_\ell) = e^{-i\mu_j(x_\ell + L)}$ and adding up ℓ from 1 to $N - 1$, we have

$$\langle -\Delta u_N, W_j \rangle_N + \langle \gamma\, u_N, W_j \rangle_N = \lambda_N \langle u_N, W_j \rangle_N.$$

Setting $u_N(x) = \sum_{j=-N/2}^{N/2-1} c_j W_j(x)$, by the orthogonality of basis $W_j(x)$, we have

$$\langle \nabla u_N, \nabla W_j \rangle_N = \sum_{k=-N/2}^{N/2-1} c_k \mu_k \mu_j \langle W_k, W_j \rangle_N = c_j \mu_j^2 = \langle -\Delta u_N, W_j \rangle_N.$$

The above identity holds true for the basis of V_N, therefore, the equivalence proof is completed. $\qquad\square$

Before introducing the convergence results, we define the following notation

$$\delta_N(u) = \inf_{v \in V_N} \left\{ \|u - v\|_1 + \sup_{w \in V_N} \frac{|a(v, w) - a_N(v, w)|}{\|w\|_1} \right\}.$$

Lemma A. 2. *Assume the $u(x)$ is a smooth and compactly supported function, i.e., $\operatorname{supp}\{u\} \subsetneq \Omega$, then the following estimate holds:*

$$\delta_N(u) \lesssim N^{-(m-\sigma)} \max\{|u|_m, |\gamma u|_m\}, \tag{A.6}$$

where $\sigma = \max\{1, d/2\}$.

Proof. From Lemma 3.1, we have

$$\|u - \mathcal{I}_N u\|_1 \lesssim N^{-(m-1)}|u|_m. \tag{A.7}$$

From the definition of X_N, we can obtain following two equations,

$$b_N(v_N, w_N) = b(v_N, w_N), \quad \langle \nabla v_N, \nabla w_N \rangle_N = \langle \nabla v_N, \nabla w_N \rangle, \quad \forall u_N, v_N \in V_N. \tag{A.8}$$

Based on (A.8), we obtain

$$\big|a(v_N, w_N) - a_N(v_N, w_N)\big| = \big|\langle \gamma v_N, w_N \rangle - \langle \gamma v_N, w_N \rangle_N\big|, \quad \forall v_N, w_N \in V_N.$$

Hence, combing $\mathcal{I}_N u \in V_N$, the following inequalities hold

$$\big|a(\mathcal{I}_N u, w_N) - a_N(\mathcal{I}_N u, w_N)\big| = \big|\langle \gamma \mathcal{I}_N u, w_N \rangle - \langle \gamma \mathcal{I}_N u, w_N \rangle_N\big|$$
$$\leq \big|\langle \gamma \mathcal{I}_N u, w_N \rangle - \langle \gamma u, w_N \rangle\big| + \big|\langle \gamma u, w_N \rangle - \langle \gamma u, w_N \rangle_N\big| + \big|\langle \gamma u, w_N \rangle_N - \langle \gamma \mathcal{I}_N u, w_N \rangle_N\big|$$
$$:= I_1 + I_2 + I_3.$$

For the first term, combing Lemma 3.1, we have

$$I_1 = \big|\langle \gamma \mathcal{I}_N u, w_N \rangle - \langle \gamma u, w_N \rangle\big| \leq \|\gamma\|_\infty \|\widetilde{u} - u\|_0 \|w_N\|_0 \lesssim N^{-m}|u|_m \|w_N\|_1.$$

Since $\operatorname{supp}\{u\} \subsetneq \Omega$, $\operatorname{supp}\{\gamma u\} \subsetneq \Omega$, γu is smooth and periodic on Ω. Setting $w_N(x) = \sum_{k=-N/2}^{N/2-1} c_k W_k(x)$, and combining [28, Theorem 2.3], the following estimates hold

$$I_2 = \big|\langle \gamma u, w_N \rangle - \langle \gamma u, w_N \rangle_N\big| \leq \sum_{k=-N/2}^{N/2-1} |c_k|\big|\langle \gamma u, W_k \rangle - \langle \gamma u, W_k \rangle_N\big|$$

$$\leq \sum_{k=-N/2}^{N/2-1} |c_k|\,|(\widehat{\gamma u})_k - (\widetilde{\gamma u})_k| \leq \sqrt{\sum_j |(\widehat{\gamma u})_j - (\widetilde{\gamma u})_j|^2}\sqrt{\sum_j |w_j|^2}$$

$$\lesssim N^{-m}|\gamma u|_m \|w_N\|_0 \leq N^{-m}|\gamma u|_m \|w_N\|_1,$$

where $(\widehat{\gamma u})_k = \int_\Omega \gamma(x)u(x)e^{-ikx}\mathrm{d}x$. For the third term, combing Lemma 3.1, we obtain

$$I_3 = \big|\langle \gamma u, w_N \rangle_N - \langle \gamma \mathcal{I}_N u, w_N \rangle_N\big| \leq \|\gamma\|_\infty \|u - \widetilde{u}\|_\infty \|w_N\|_0 \lesssim N^{-(m-d/2)}|u|_m \|w_N\|_1.$$

Based on the definition of $\delta_N(u)$ and above error estimates, we have

$$\delta_N(u) \lesssim N^{-(m-1)}|u|_m + N^{-m}|u|_m + N^{-m}|\gamma u|_m + N^{-(m-d/2)}|u|_m$$
$$\lesssim N^{-(m-\sigma)} \max\{|u|_m, |\gamma u|_m\}.$$

$\square$

Based on (A.2) and the general theory of the error estimates for the eigenvalue problems by the approximation method [1, Section 8] and [28, Section 1], we have the following convergence results.

Lemma A.3. *For any eigenpair approximation (λ_N, u_N) of (A.4), there is an eigenpair (λ, u) of (A.3) corresponding to λ such that*

$$\|u - u_N\|_1 \lesssim \delta_N(u), \quad \|u - u_N\| \lesssim \zeta_N \|u - u_N\|_1, \quad |\lambda - \lambda_N| \lesssim \|u - u_N\|_1^2,$$

where $\zeta_N \to 0$ as $N \to \infty$.

References

[1] I. Babuška, J. E. Osborn, *Eigenvalue Problems*, Handbook of Numerical Analysis, Vol. II, Finite Element Methods, North-Holland, Amsterdam, (1991).

[2] Z. Bai and R.C. Li., *Minimization principles for the linear response eigenvalue problem I: Theory*, SIAM J. Matrix Anal. Appl., **33**(4) (2012), 1075–1100.

[3] Z. Bai and R.C. Li, *Minimization principles for linear response eigenvalue problem II: Computation*, SIAM J. Matrix Anal. Appl., **34**(2) (2013), 392–416.

[4] D. Baillie, R.M. Wilson and P.B. Blakie, *Collective excitations of self-bound droplets of a dipolar quantum fluid*, Phys. Rev. Lett., **119**(25) (2017), article 255302.

[5] W. Bao and Y. Cai, *Mathematical models and numerical methods for spinor Bose-Einstein condensates*, Commun. Comput. Phys., **24**(4) (2018), 899–965.

[6] W. Bao and H. Wang, *A mass and magnetization conservative and energy-diminishing numerical method for computing ground state of spin-1 Bose-Einstein condensates*, SIAM J. Numer. Anal., **45**(5) (2007), 2177–2200.

[7] I. Bloch, J. Dalibard and W. Zwerger, *Many-body physics with ultracold gases*, Rev. Mod. Phys., **80**(3) (2008), 885–964.

[8] E. Cancés, R. Chakir and Y. Maday, *Numerical analysis of nonlinear eigenvalue problems*, J. Sci. Comput., **45** (2010), 90–117.

[9] L. Chen, H. Pu, Z.-Q. Yu and Y. Zhang, *Collective excitation of a trapped Bose-Einstein condensate with spin-orbit coupling*, Phys. Rev. A, **95**(3) (2017), article 033616.

[10] I. Danaila, M.A. Khamehchi, V. Gokhroo, P. Engels and P.G. Kevrekidis, *Vector dark-anti dark solitary waves in multicomponent Bose-Einstein condensates*, Phys. Rev. A, **94**(5) (2016), article 053617.

[11] S.-X. Deng, T. Shi and S. Yi, *Spin excitations in dipolar spin-1 condensates*, Phys. Rev. A, **102**(1) (2020), article 013305.

[12] M. Edwards, P.A. Ruprecht, K. Burnett, R.J. Dodd and C.W. Clark, *Collective excitations of atomic Bose-Einstein condensates*, Phys. Rev. Lett., **77**(9) (1996), 1671–1674.

[13] Y. Gao and Y. Cai, *Numerical methods for Bogoliubov-de Gennes excitations of Bose-Einstein condensates*, J. Comput. Phys., **403** (2020), article 109058.

[14] D.S. Hall, M.R. Matthews, J.R. Ensher, C.E. Wieman and E.A. Cornell, *Dynamics of component separation in a binary mixture of Bose-Einstein condensates*, Phys. Rev. Lett., **81**(8) (1998), 1539–1542.

[15] T.-L. Ho, *Spinor Bose condensates in optical traps*, Phys. Rev. Lett., **81**(4) (1998), 742–745.

[16] B. Hu, G. Huang and Y. Ma, *Analytical solutions of the Bogoliubov–de Gennes equations for excitations of a trapped Bose-Einstein-condensed gas*, Phys. Rev. A, **69**(6) (2004), article 063608.

[17] J.A.M. Huhtamäki and P. Kuopanportti, *Elementary excitations in dipolar spin-1 Bose-Einstein condensates*, Phys. Rev. A, **84**(4) (2011), article 043638.

[18] L. Jia, A.-B. Wang and S. Yi, *Low-lying excitations of vortex lattices in condensates with anisotropic dipole-dipole interaction*, Phys. Rev. A, **97** (2018), article 043614.

[19] D.S. Jin, J.R.Ensher, M.R. Matthews, C.E. Wieman and E.A. Cornell, *Collective excitations of a Bose-Einstein condensate in a dilute gas*, Phys. Rev. Lett., **77**(3) (1996), 420–423.

[20] Y. Kawaguchi and M. Ueda, *Spinor Bose-Einstein condensates*, Phys. Rep., **520**(5) (2012), 253–381.

[21] Y. Li, Z. Wang and Y. Zhang, *A Bi-Orthogonal Structure-Preserving eigensolver for large-scale linear response eigenvalue problem*, preprint.

[22] W. Liu and Y. Cai, *Normalized gradient flow with Lagrange multiplier for computing ground states of Bose-Einstein condensates*, SIAM J. Sci. Comput., **43**(1) (2021), B219–B242.

[23] X. Liu, Q. Tang, S. Zhang and Y. Zhang, *On optimal zero padding of kernel truncation method*, SIAM J. Sci. Comput., **46**(1) (2024), A23–A49.

[24] M.R. Matthews, D.S. Hall, D.S. Jin, J.R. Ensher, C.E.Wieman, E.A. Cornell, F. Dalfovo, C. Minniti and S. Stringari, *Dynamical response of a Bose-Einstein condensate to a discontinuous change in internal state*, Phys. Rev. Lett., **81**(2) (1998), 243–247.

[25] T. Ohmi and K. Machida, *Bose-Einstein Condensation with internal degrees of freedom in alkali atom gases*, J. Phys. Soc. Jpn., **67** (1998), 1822–1825.

[26] G. Sadaka, V. Kalt, I. Danaila and Frédéric Hecht, *A finite element toolbox for the Bogoliubov-de Gennes stability analysis of Bose-Einstein condensates*, Comput. Phys. Commun., **294** (2024), article 108948.

[27] M. Shao, F. H. da Jornada, L. Lin, C. Yang, J. Deslippe and S. G. Louie, *A structure preserving Lanczos algorithm for computing the optical absorption spectrum*, SIAM J. Matrix Anal. Appl., **39**(2) (2018), 683–711.

[28] J. Shen, T. Tang and L.-L. Wang, *Spectral Methods: Algorithms, Analysis and Applications*, Springer, (2011).

[29] D.M. Stamper-Kurn, M.R. Andrews, A.P. Chikkatur, S.Inouye, H.-J. Miesner, J. Stenger and W. Ketterle, *Optical confinement of a Bose-Einstein condensate*, Phys. Rev. Lett., **80**(10) (1998), 2027–2030.

[30] D.M. Stamper-Kurn and M. Ueda, *Spinor Bose gases: Symmetries, magnetism and quantum dynamics*, Rev. Modern Phys., **85**(3) (2013), 1191–1244

[31] J. Stenger, S. Inouye, D.M. Stamper-Kurn, H.-J. Miesner, A.P. Chikkatur and W. Ketterle, *Spin domains in ground-state Bose-Einstein condensates*, Nature, **396**(6709) (1998), 345–348.

[32] S. Stringari, *Collective excitations of a trapped Bose-condensed gas*, Phys. Rev. Lett., **77**(12) (1996), 2360–2363.

[33] Q. Tang, M. Xie, Y. Zhang and Y. Zhang, *A spectrally accurate numerical method for computing the Bogoliubov-de Gennes excitations of dipolar Bose-Einstein condensates*, SIAM J. Sci. Comput., **44**(1) (2022), B100–B121.

[34] *The ARPACK homepage. https://www.caam.rice.edu/software/ARPACK/*

[35] T. Tian, Y. Cai, X. Wu and Z. Wen, *Ground states of spin-F Bose-Einstein condensates*, SIAM J. Sci. Comput., **42**(4) (2020), B983–B1013.

[36] R.M. Wilson, S. Ronen and J.L. Bohn, *Stability and excitations of a dipolar Bose-Einstein condensate with a vortex*, Phys. Rev. A, **79**(1) (2009), article 013621.

[37] W. Zhang, S. Yi and L. You, *Mean field ground state of a spin-1 condensate in a magnetic field*, New J. Phys., **5**(1) (2003), article 77.

[38] Y. Zhang, X. Liu and M. Xie, *Efficient and accurate computation of the Bogoliubov-de Gennes excitations for the quasi-2D dipolar Bose-Einstein Condensates*, East Asian J. Appl. Math., **11**(4) (2021), 686–707.